

11-2019

## Active Filter Modelling To Mitigate Harmonics Generated By Electric Vehicle Chargers

Fasalu Rahman Puthiyottil

Follow this and additional works at: [https://scholarworks.uaeu.ac.ae/electric\\_theses](https://scholarworks.uaeu.ac.ae/electric_theses)



Part of the [Engineering Commons](#)

---

### Recommended Citation

Puthiyottil, Fasalu Rahman, "Active Filter Modelling To Mitigate Harmonics Generated By Electric Vehicle Chargers" (2019). *Electrical Engineering Theses*. 6.  
[https://scholarworks.uaeu.ac.ae/electric\\_theses/6](https://scholarworks.uaeu.ac.ae/electric_theses/6)

This Thesis is brought to you for free and open access by the Electrical Engineering at Scholarworks@UAEU. It has been accepted for inclusion in Electrical Engineering Theses by an authorized administrator of Scholarworks@UAEU. For more information, please contact [fadl.musa@uaeu.ac.ae](mailto:fadl.musa@uaeu.ac.ae).

**UAEU**



جامعة الإمارات العربية المتحدة  
United Arab Emirates University

United Arab Emirates University

College of Engineering

Department of Electrical Engineering

**ACTIVE FILTER MODELLING TO MITIGATE HARMONICS  
GENERATED BY ELECTRIC VEHICLE CHARGERS**

Fasalu Rahman Puthiyottil

This thesis is submitted in partial fulfilment of the requirements for the degree of  
Master of Science in Electrical Engineering

Under the Supervision of Dr. Hussain Shareef

November 2019

### Declaration of Original Work

I, Fasalu Rahman Puthiyottil, the undersigned, a graduate student at the United Arab Emirates University (UAEU), and the author of this thesis entitled "*Active Filter Modelling to Mitigate Harmonics Generated by Electric Vehicle Chargers*", hereby, solemnly declare that this thesis is my own original research work that has been done and prepared by me under the supervision of Dr. Hussain Shareef, in the College of Engineering at UAEU. This work has not previously been presented or published, or formed the basis for the award of any academic degree, diploma or a similar title at this or any other university. Any materials borrowed from other sources (whether published or unpublished) and relied upon or included in my thesis have been properly cited and acknowledged in accordance with appropriate academic conventions. I further declare that there is no potential conflict of interest with respect to the research, data collection, authorship, presentation and/or publication of this thesis.

Student's Signature: \_\_\_\_\_



Date: \_\_\_\_\_

12/02/2020

## Approval of the Master Thesis

This Master Thesis is approved by the following Examining Committee Members:

- 1) Advisor (Committee Chair): Dr. Hussain Shareef

Title: Associate Professor

Department of Electrical Engineering

College of Engineering

Signature  \_\_\_\_\_

Date 30/01/2020

- 2) Member: Dr. Rachid Errouissi

Title: Assistant Professor

Department of Electrical Engineering

College of Engineering

Signature  \_\_\_\_\_

Date 30/01/2020

- 3) Member (External Examiner): Dr. Mithulananthan Nadarajah

Title: Associate Professor

Department of Electrical Engineering.


School of Information Technology and Electrical Engineering, Australia

Signature  \_\_\_\_\_


Date 30/01/2020

This Master Thesis is accepted by:

Dean of the College of Engineering: Professor Sabah Alkass

Signature  Date 12/2/2020

Dean of the College of Graduate Studies: Professor Ali Al-Marzouqi

Signature  Date 13/2/2020

Copy 1 of 4

Copyright © 2019 Fasalu Rahman Puthiyottil  
All Rights Reserved

## Abstract

The Automotive industry is going through a rapid transformation to adopt electrified technology. A major share of the electrified vehicles is going to be in the Battery electric vehicles (BEVs) and plug in hybrids segments that need to connect to the grid to recharge the batteries. For customer convenience, the time required for fully charging the battery need to be brought down significantly. EV charging stations are getting installed that could bring down the charging time to less than 30 minutes. However this pose a unique issue to the power quality of the utility grid. During charging, the EV charging unit injects harmonics to the grid. When a large number of EVs are getting charge simultaneously, which is a likely scenario in the future, the degradation in the power quality of the grid would be significant. This thesis discuss the modelling of an active filter to reduce the Total harmonic distortion (THD) generated by electric vehicle (EV) chargers. The main objective of this thesis is to determine the percentage of harmonic current injected by the EV chargers to the power grid and to model an active filter to mitigate the harmonic distortion generated by these chargers. The active filter is modelled as bidirectional three-phase pulse width modulation (PWM) rectifier. The EV in this proposed model is represented as an injected current harmonic source. Positive sequence synchronous reference frame controller (SRFC) is used to generate the reference current. The hysteresis controller is used to compare the load current and injected current, and its output is used to generate the switching pulses for Metal oxide semiconductor field effect transistor (MOSFET). The DC link voltage control is achieved by using conventional Proportional and integral controller (PI) and fuzzy logic control PI. MATLAB/Simulink simulation result shows that the proposed filter can be used to mitigate the THD of EV chargers without violating the limit set by IEEE Std. 519-1992.

**Keywords:** Total Harmonic Distortion, Electric vehicle, SRFC, Fuzzy PI, Hysteresis controller, MOSFET.

## Title and Abstract (in Arabic)

### نمذجة مرشح نشط لتخفيض التشوه التوافقي الناشئ من شواحن السيارات الكهربائية

#### الملخص

مجال صناعة السيارات يمر بتحول متسارع نحو اعتماد تكنولوجيا الطاقة الكهربائية. النصيب الأكبر في مجال السيارات الكهربائية سيكون للسيارات الكهربائية التي تستخدم البطارية (BEV) و أيضا من نصيب الاجزاء الهجينة في السيارة التي توصل بشبكة الكهرباء بغرض شحن البطارية. من المناسب للمستخدمين ان يكون الزمن اللازم لشحن البطارية أقل ما يمكن . المحطات اللازمة لشحن البطاريات يمكن أن تخفض زمن الشحن ليكون أقل من 30 دقيقة، من جهة أخرى، هذا يضيف مزيد من التحديات على جودة الطاقة الموجودة في الشبكة الكهربائية العامة . عندما يتم شحن عدد كبير من السيارات الكهربائية بصورة متزامنة و هو سيناريو محتمل في المستقبل سيؤثر ذلك على جودة الطاقة المقدمة من الشبكة بصورة كبيرة .

في هذا البحث نناقش نمذجة مرشح نشط (Active Filter) بغرض تخفيض التشوه التوافقي (Total harmonic distortion) الناشئ من شواحن السيارات الكهربائية . إن الهدف الأساسي من هذا البحث هو تحديد نسبة التشوه التوافقي الناشئ من شواحن السيارات الكهربائية مؤثرا على الشبكة العامة بالاضافة الى نمذجة مرشح نشط قادر على مجابهة هذا التشوه . تم نمذجة المرشح النشط كمقوم لتعديل عرض النبضة الثلاثي ثنائي الإتجاه.

إنَّ السيارة الكهربائية في هذا النموذج تمثل مصدرا للتيار التوافقي، و متحكم سلسلة الحزمة المتوافقة المرجعية (SRFC) يستخدم لتوليد التيار المرجعي . متحكم التباطؤ (Hysteresis Controller) يستخدم لمقارنة تيار الحمل بالتيار المرجعي و ما ينتج عنه يستخدم لتوليد نبضات تشغيل للترانزستور (MOSFET) . التحكم في وصلة الجهد المستمر يتم تنفيذه عن طريق استخدام متحكم تكاملي (PI) و متحكم منطق ضبابي (Fuzzy logic control). نتائج المحاكاة في برنامج الماتلاب (MATLAB/Simulink) ظهرت أن المرشح المقترح يمكن استخدامه لمجابهة التشوه التوافقي لشواحن السيارات الكهربائية دون أن يتم الإخلال بالحدود الموضوعة في مواصفة IEEE 519-1992.



**مفاهيم البحث الرئيسية:** تخفيض التشوه التوافقي، سيارة الكهرباء، للترانزستور، مرشح نشط ،  
متحكم منطق ضبابي.

## **Acknowledgments**

I would like to express my deepest gratitude to my thesis supervisor Dr. Hussain Shareef of the department of Electrical engineering at UAE University. His patience, motivation, enthusiasm, immense knowledge and his guidance helped me in all the time of research and writing of this thesis.

Besides my advisor, I would like to thank Dr. Mousa Hussain for his continuous support. I also thank my fellow classmate Mr. Mohamed Asker, Mr. Nakul Narayanan for their continuous support, motivation, stimulating discussions and for all the fun we have had in the last three years.

Last but not the least, I would like to thank my wife Ms. Najiya, my son Hamiz and my parents for supporting me during my study at UAEU.

## **Dedication**

*To my beloved parents and family*

## Table of Contents

Title .....	i
Declaration of Original Work .....	ii
Copyright .....	iii
Approval of the Master Thesis .....	iv
Abstract .....	vi
Title and Abstract (in Arabic) .....	vii
Acknowledgments .....	ix
Dedication .....	x
Table of Contents .....	xi
List of Tables .....	xiii
List of Figures .....	xiv
List of Abbreviations .....	xvi
Chapter 1: Introduction .....	1
1.1 Overview .....	1
1.2 EV charger power levels .....	4
1.2.1 Level 1 charging .....	4
1.2.2 Level 2 charging .....	5
1.2.3 Level 3 charging .....	5
1.3 Harmonic calculation .....	6
1.3.1 Harmonic limits .....	8
1.3.2 Total demand distortion (TDD) .....	10
1.4 Non-linear load modeling .....	10
1.5 Harmonic mitigation methods .....	12
1.5.1 Passive filters .....	14
1.5.2 Active filters .....	14
1.5.3 Hybrid filters .....	15
1.6 Active filter .....	15
1.6.1 Series active filter .....	15
1.6.2 Parallel (shunt) active filter (PAF) .....	16
1.6.3 Combination of PAF and SAF .....	17
1.7 PAF .....	18
1.7.1 Working principle of VSI .....	20
1.7.2 Three-phase VSI .....	22
1.8 Power factor correction (PFC) converters .....	24
1.8.1 Comparison of PFC converter topologies .....	25

1.9 Control strategies for shunt active filter.....	26
1.9.1 Constant Instantaneous power technique.....	26
1.9.2 Generalized fryze currents minimization technique.....	27
1.9.3 Synchronous reference frame controller (SRFC).....	28
1.10 Fuzzy logic controller (FLC) .....	29
1.10.1 Fuzzification.....	29
1.10.2 Knowledgebase .....	30
1.10.3 Fuzzy inference engine.....	30
1.10.4 De-Fuzzification.....	30
1.11 Problem Statement .....	31
1.12 Objective .....	32
1.13 Scope of the work .....	32
Chapter 2: Development of Active Filter for Harmonic Elimination .....	33
2.1 Proposed EV charger model.....	33
2.2 Features of the parallel active filter.....	38
2.2.1 Harmonic producing nonlinear loads .....	38
2.3 Voltage source inverter connected to EV charger.....	42
2.4 Filter control.....	43
2.4.1 Phase locked loop (PLL) .....	43
2.4.2 ABC to dq0 transform .....	44
2.5 Synchronous reference frame controller (SRFC).....	45
2.5.1 VSI with positive sequence SRFC .....	46
2.6 DC link voltage control.....	49
2.7 Fuzzy PI controller.....	51
2.7.1 Mamdani's method.....	52
2.8 Hysteresis controller .....	55
Chapter 3: Results and Discussion.....	59
3.1 Performance of VSI in various condition.....	67
Chapter 4: Conclusion.....	75
References.....	76

**List of Tables**

Table 1: EV charger specification.....	2
Table 2: IEEE Std. 519-1992 harmonic voltage limits .....	8
Table 3: IEEE Std. 519-1992 harmonic current limits.....	9
Table 4: Harmonic mitigation circuit topologies .....	13
Table 5: Switching states and output voltage of single phase inverter .....	21
Table 6: Line current harmonic content of an EV charger.....	35
Table 7: Grid modeling parameters.....	37
Table 8: Rule base for determining $K_p1$ .....	55
Table 9: Table base for determining $K_i1$ .....	55
Table 10: Comparison of the control strategy.....	74

## List of Figures

Figure 1: Single phase unidirectional multilevel charger unit .....	5
Figure 2: Three phase full bridge bidirectional charger.....	6
Figure 3: Distorted waveform .....	7
Figure 4: EVs connected to the grid.....	10
Figure 5: Current waveform of the non - linear load .....	11
Figure 6: THD at source side due to a non-linear load .....	11
Figure 7: Series Active filter .....	16
Figure 8: Parallel Active filter .....	16
Figure 9: Combination of series and parallel active filter.....	18
Figure 10: Block diagram of parallel active filter .....	18
Figure 11: PWM current source inverter (CSI).....	19
Figure 12: PWM voltage source inverter .....	19
Figure 13: Single phase voltage source inverter .....	20
Figure 14: Single phase VSI circuit diagram .....	21
Figure 15: 3phase VSI.....	22
Figure 16: Switching patterns of 3-phase VSI .....	23
Figure 17: Phase and line voltage output of 3phase VSI .....	23
Figure 18: Power factor correction with HF isolation .....	24
Figure 19: Block diagram of constant instantaneous power method .....	27
Figure 20: Fryze current control block diagram .....	28
Figure 21: Block diagram of fuzzy logic controller.....	29
Figure 22: EV harmonic model.....	34
Figure 23: Three phase load current of an EV charger .....	35
Figure 24: Circuit diagram model of an EV charger.....	36
Figure 25: THD at the source side .....	38
Figure 26: Norton equivalent harmonic current source .....	39
Figure 27: Norton equivalent circuit with PAF.....	40
Figure 28: EVs with VSI.....	42
Figure 29: PLL block diagram .....	43
Figure 30: ABC to DQ transformation.....	45
Figure 31: Voltage source inverter circuit model .....	46
Figure 32: Filter control .....	47
Figure 33: Connection diagram of positive sequence SRFC .....	48
Figure 34: Connection diagram of neutral current compensation.....	49
Figure 35: Capacitor voltage control.....	49
Figure 36: Load side THD .....	50
Figure 37: Source side THD .....	51
Figure 38: Block diagram of fuzzy PI.....	53
Figure 39: Fuzzy PI for DC link voltage control .....	53

Figure 40: Membership function of inputs (error & change of error).....	54
Figure 41: Membership function of outputs (Kp1 and Ki1) .....	54
Figure 42: Hysteresis band controller .....	56
Figure 43: Hysteresis current control.....	57
Figure 44: Hysteresis current regulator.....	58
Figure 45: Load current waveform .....	59
Figure 46: Grid current waveform of PAF with normal PI.....	60
Figure 47: Grid current THD .....	60
Figure 48: Connection diagram of EV load with VSI.....	62
Figure 49: Filter control .....	63
Figure 50: Filter converter .....	64
Figure 51: THDi of EV charger connected to VSI with fuzzy PI.....	65
Figure 52: DC link voltage control .....	66
Figure 53: Reference current tracking.....	66
Figure 54: Load current waveform of PAF with fuzzy PI .....	67
Figure 55: Grid current waveform of PAF with fuzzy PI .....	67
Figure 56: THDi at load side when an additional EV connected to R phase .....	68
Figure 57: THDi at source side when an additional EV connected to R phase.....	68
Figure 58: DC link voltage control when an additional EV plugged into R phase.....	69
Figure 59: Neutral current compensation.....	69
Figure 60: THDi at load side when two additional EVs are plugged into the system .....	70
Figure 61: THDi at source side when two additional EVs are plugged into the system .....	70
Figure 62: DC link voltage when two additional EVs are plugged at 0.45s .....	71
Figure 63: Diode rectifier connected to active filter .....	71
Figure 64: Current waveform on the R phase .....	72
Figure 65: DC link voltage when diode rectifier connected .....	72
Figure 66: THDi at load side.....	73
Figure 67: THDi at the grid side when diode rectifier connected.....	73



### List of Abbreviations

COG	Center of Gravity
EV	Electric Vehicle
FFT	Fast Fourier Transform
FIS	Fuzzy Inference System
FIS	Fuzzy Inference System
FLC	Fuzzy Logic Controller
IEEE	Institute of Electrical and Electronics Engineers
Irms	Root Mean Square Current
Ki	Integral Gain
Kp	Proportional Gain
LPF	Low Pass Filter
LV	Low Voltage
MF	Membership Function
MF	Membership Function
MOM	Mean of Maximum
MOSFET	Metal Oxide Semiconductor Field Effect Transistor
PI	Proportional + Integral
PLL	Phase Locked Loop
PWM	Pulse Width Modulation
SOC	State of Charge
SRFC	Synchronous Reference Frame Controller
TDD	Total Demand Distortion
THD	Total Harmonic Distortion
Vrms	Root Mean Square Voltage
VSI	Voltage Source Inverter

## **Chapter 1: Introduction**

### **1.1 Overview**

Over the last decade, an increasing number of car owners have been choosing electric vehicles (EVs) to replace gasoline vehicles. These EVs are expected to become considerably popular in the coming years. The popularity of EVs has increased due to their overall fuel efficiency, zero carbon emission, and low-cost maintenance. Moreover, the attractive incentives offered by government entities reduce the prices of EVs. A pure electric car with an onboard power storage unit does not produce greenhouse gas emissions. Hence, the importance of such type of vehicle continues to increase. These EVs require a large amount of power to charge their batteries (Shao, Pipattanasomporn, & Rahman, 2011). When fully charged, EVs provide a satisfactory range to their owners. However, during the charging process, EV chargers negatively affect the power system grid through harmonic distortion, overheating, and overloading of transformers. Therefore, maintaining power quality terms such as voltage fluctuations, total harmonic distortions (THDs), and changes in frequencies within the standard limits set is important.

EV chargers are used to charge battery packs from the grid. An EV consists of several power electronic components, such as a battery and battery charger, an induction motor and its control, and a power train. Evidently, during EV charging, the voltage profile of the grid becomes distorted due to the injection of harmonic current. This harmonic current leads to increased line losses, overloading of cables, and overheating of transformers. These conditions cause a gradual decrease in the life span of motors, transformers, and generators. Thus, determining the percentage of harmonic

content injected by these chargers is highly important. In addition, installing harmonic mitigation techniques within charging stations is essential to maintain THDs within the allowable limit.

EV chargers can be classified according to their power levels, namely, Levels 1, 2, and 3 (Yilmaz & Krein, 2012). These charging power levels are shown in Table-1. Level 1 (slow) charging is available at home; it requires a single-phase supply. Level 2 charging is considered the main method for public and private facilities; it requires a 240 V outlet. Level 3 charging, as well as DC fast charging, requires a three-phase supply. Level 3 EV chargers are intended for commercial use, and they operate similar to gas station chargers. These chargers require 20–30 min to recharge EV battery packs. A brief description of EV charger power is presented in the following section.

Table 1: EV charger specification

Power level Types	Charger Location	Typical Use	Energy Supply interface	Expected power level	Charging time	Vehicle Technology
Level 1 (Opportunity) 120 Vac (US) 230Vac(EU)	On board 1 phase	Charging at home or office	Convenience outlet	1.4kW 1.9kW	4-11 hours 11-36 hours	PHEVs(5-15kWh) EVs(16-50 kWh)
Level 2(Primary) 240 Vac(US) 400 Vac(EU)	On board 1 or 3 phase	Charging at private or public outlets	Dedicated EVSE	4kW 8kW 19.2kW	1-4 hours 2-6 hours 2-3 hours	PHEVs(5-15 kWh) EVs(16-30 kWh) EVs(3-50 kWh)
Level 3 (Fast) 208-600Vac or Vdc	Off-board 3phase	Commercial, analogues to filling station	Dedicated EVSE	50kW 100kW	0.4-1hour 0.2-0.5hour	EVs(20-50 kWh)

Modern EV battery chargers contain boost converters for active power factor correction (PFC) (Lee, Jeong, Lee, & Hur, 2011). They are used to improve the power factor on the basis of harmonic current regulation limits, and the maximum power factor is 0.99. In the current study, the switching noise generated by the switch and diode is reduced. In addition, a resonant-type phase shift full bridge is used for power

conversion. A detailed study of various PFCs of EV chargers is explained at the end of this chapter.

The author of (Deilami, 2018) explained the smart grid's performance and power quality effects due to the uncoordinated charging of EV batteries. This study revealed unacceptable THDs. Hence, the author suggested that coordinated charging improves power quality problems. However, a well-coordinated approach and detailed power system studies remain necessary.

In some instances, harmonic distortions decrease considerably when different types of EVs are connected to the grid for charging. As a result of the diversity of charging methods, the overall distortion produced is lower than the highest level of distortion produced by individual chargers (Kutt, Saarijarvi, Lehtonen, Molder, & Niitsoo, 2013; Guo et al., 2018). However, nowadays each car manufacturers has their own charging technology adopted in their charging stations. The simultaneous operation of several 1-phase chargers in the same Low voltage (LV) feeder, with maximum 3rd harmonic currents around 12% and THDi between 12% and 16%, can have a significant impact on distribution networks (Melo, Mira, de Almeida, & Delgado, 2011). Due to this, it will distort current and voltage waveforms. So modeling of an active filter for an EV charger will be very useful to analyze the extent at which it distorted the current waveform.

Harmonic problems in the power grid can be solved using suitable circuit topology or appropriate filters. A detailed study on commonly used circuit topologies and different types of filters is discussed in the following section of this chapter. A voltage source inverter (VSI) and its drive circuit are commonly used to mitigate the

harmonic currents in the grid. A recent study showed that this VSI based on an active power filter with constant frequency integration control can be used to compensate for harmonic currents (Wenjin Dai, Baofu Wang, & Hua Yang, 2009).

Thus, the current work develops a MATLAB/Simulink simulation to demonstrate the THD-I mitigation of VSIs during simultaneous EV charging. A comparative study of VSIs is conducted with two different control methods, namely, using a positive sequence synchronous reference frame controller (SRFC) with normal proportional–integral (PI) control and using fuzzy PI controller.

In the next section, charger power levels, standards, and terms related harmonic problems are explained in detail.

## **1.2 EV charger power levels**

The abundance of charging infrastructure reduces the battery requirement, weight, and cost of an EV. We can broadly classify EV chargers into three types according to power levels, as described in the following section.

### **1.2.1 Level 1 charging**

Level 1 charging is the slowest among all levels, and chargers of this type are best suited for overnight use at a garage or at home. The power level for this type is less than 2 kW, and it uses a standard 120 V/15 A single-phase earthed supply. Hence, this type of charger requires no additional installation. The approximate total investment cost on the charging station for a Level 1 charger is \$500–\$880 (Yilmaz & Krein, 2013).

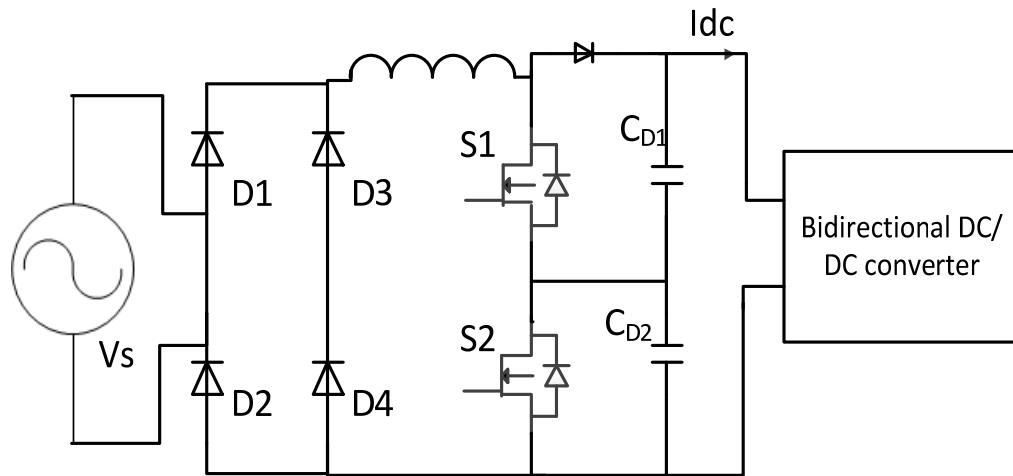


Figure 1: Single phase unidirectional multilevel charger unit

### 1.2.2 Level 2 charging

This type of charging is applicable to public car parking stations and shopping malls. Chargers of this type work with 240 V AC supply. This charging method requires one dedicated equipment and a connection installation. Some EV manufacturers provide the required power electronics onboard. Hence, only a power outlet is required. The popularity of this type of charger among EV owners has increased because of its rapid charging time. The approximate investment cost for this type of charger is less than \$3000. Figure 1 shows the common circuit topology used for single-phase unidirectional multilevel chargers for Levels 1 and 2 charging (Yilmaz & Krein, 2012)

### 1.2.3 Level 3 charging

Level 3 EV charging stations differs from level 1 and 2 chargers in that the rectification is takes place in the charger itself. This helps to supply high current to EV power pack in a short interval of time. Given the rapid charging at this level, EV battery charging can be completed in less than 1 hour. This type of charger requires a three-

phase supply and an external charger to provide a regulated DC supply because of its high charging rate. The approximate investment cost for this type of charging station is in between \$30K and \$160K. Figure 2 shows a three-phase bidirectional DC to DC converter. In addition to high power levels, this converter can provide reduced THDs, high power factors, and ripple-free output DC supply. Hence, Level 3 chargers are most suitable for the fast charging of EVs. This type of charger requires pulse width modulation (PWM) inputs, which in turn increases the complexity and cost of circuits (Yilmaz & Krein, 2012).

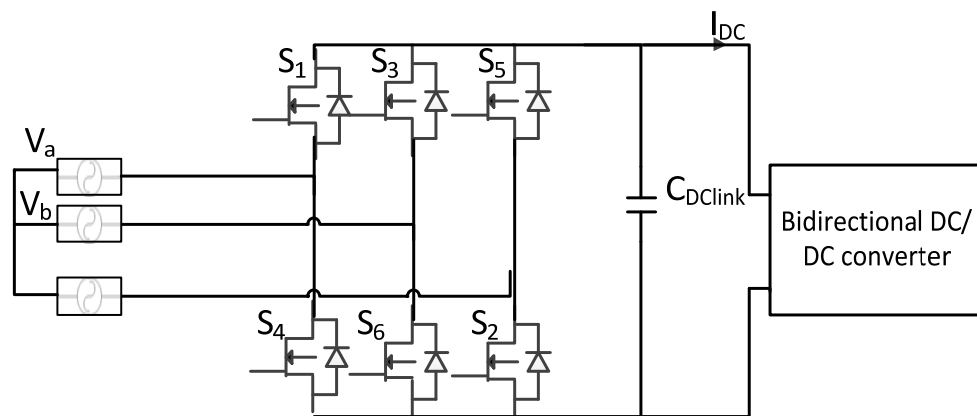


Figure 2: Three phase full bridge bidirectional charger

### 1.3 Harmonic calculation

IEEE Std. 519-1992 – IEEE Recommended Practices and Requirements for Harmonic Control in Electric Power systems provides a groundwork for harmonic limits (Blooming & Carnovale, 2006). Harmonic is “A sinusoidal component of a periodic wave or quantity having a frequency that is an integral multiple of the fundamental frequency” and it can be calculated as a square root of the sum of the squares of different frequency components.

For example, 10 A, 50 Hz current combined with 2 A 3<sup>rd</sup> (3x50=150 Hz) & 1 A 5<sup>th</sup> (250 Hz) harmonic current respectively, Harmonic current  $=\sqrt{10^2 + 2^2 + 1^2}$ , adds up to 10.246 A<sub>RMS</sub>.

The non-linear load connected to a power system generates non – sinusoidal current, which causes distortion in voltage drop. This distorted current can be represented as a sum of different sinusoidal current components having multiples of fundamental frequencies.

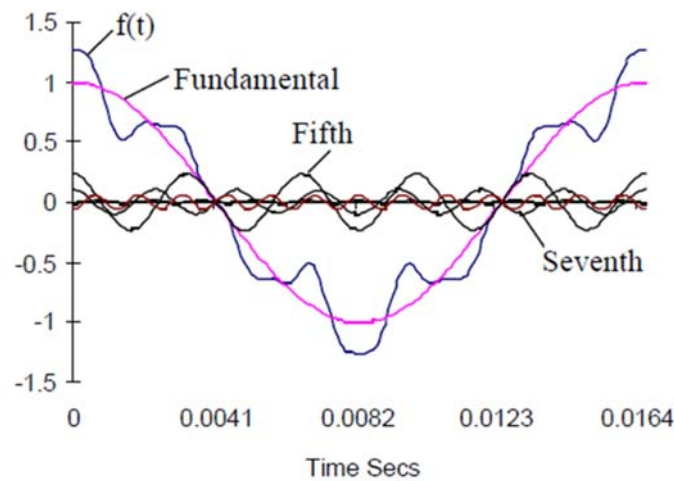


Figure 3: Distorted waveform

Figure 3 shows the waveform of a typical non-linear load. Due to the presence of harmonics, the fundamental wave becomes distorted and its final shape denoted as function  $f(t)$ . By using Fourier theory, we can extract fundamental current from it. Usually, the distortion level can be represented by the term called total harmonic distortion (THD). Total current and voltage harmonic distortion can be calculated as

$$\text{THDi} = \frac{\sqrt{\sum_{h=2}^H I_h^2}}{I_1} \cdot 100 \%, \quad (1.1)$$



$$\text{THD}_V = \frac{\sqrt{\sum_{h=2}^H V_h^2}}{V_1} \cdot 100 \% \quad (1.2)$$

Where h represents harmonic order, 'h' is the highest number of harmonic.

### 1.3.1 Harmonic limits

The harmonic voltage and current distortion on a power system are tabulated (Tables 2 and 3) on the basis of IEEE 519. As per this standard, the individual voltage distortion and THD allowed on power systems of 69 kV and below are 3% and 5%, respectively. Harmonic current distortion depends on the short circuit capacity of the system at the point of common coupling (PCC). Table 3 shows that if the ratio of  $I_{sc}/I_L$  at the PCC increases, then the power system can handle more harmonic currents; thus, a customer is allowed to inject more harmonic currents.

Table 2: IEEE Std. 519-1992 harmonic voltage limits

Voltage Distortion Limits		
Bus Voltage at PCC	Individual Voltage Distortion (%)	Total Voltage Distortion THD (%)
Below 69 kV	3.0	5.0
69 kV to 161 kV	1.5	2.5
161 kV and above	1.0	1.5

Table 3: IEEE Std. 519-1992 harmonic current limits

Maximum Harmonic Current Distortion in Percent of $I_L$						
Individual Harmonic Order (Odd Harmonics)						
$I_{sc}/I_L$	$<11$	$11 \leq h < 17$	$17 \leq h < 23$	$23 \leq h < 35$	$\geq 35$ h	TDD
$<20^*$	4.0	2.0	1.5	0.6	0.3	5.0
$20 < 50$	7.0	3.5	2.5	1.0	0.5	8.0
$50 < 100$	10.0	4.5	4.0	1.5	0.7	12.0
$100 < 1000$	12.0	5.5	5.0	2.0	1.0	15.0
$>1000$	15.0	7.0	6.0	2.5	1.4	20.0
Even harmonics are limited to 25% of the odd harmonic limits above.						
Current distortions that result in a dc offset, e.g. half-wave converters, are not allowed.						
* All power generation equipment is limited to these values of current distortion, regardless of actual $I_{sc}/I_L$ .						

Where,

$I_{sc}$  = maximum short-circuit current at PCC.

$I_L$  = maximum demand load current (fundamental frequency component) at PCC

TDD = Total demand distortion (RSS), harmonic current distortion in % of maximum demand load current (15 or 30 min demand).

### 1.3.2 Total demand distortion (TDD)

As per IEEE 519 standard, the definition of TDD is harmonic distortion in % of maximum demand load current (15 or 30 min demand). It can be calculated as shown in the Equation 1.3.

$$\text{TDDi} = \frac{\sqrt{I_2^2 + I_3^2 + I_4^2 + I_5^2 + \dots}}{I_L} \quad (1.3)$$

Where  $I_1, I_2, I_3, \dots$  Are harmonic currents.  $I_1$  refers to current at the fundamental frequency (50 Hz), and  $I_2$  second harmonic current or twice the fundamental frequency, or  $2 \times 50 = 100$  Hz. And so on.

### 1.4 Non-linear load modeling

The injection of harmonic currents in the power grid method is aimed at simulating the effects of EV chargers on the power grid. The harmonic current profile of a commercially available EV is used to model the harmonic current source. To simulate three EVs plugged into the power system, the harmonic current's magnitude and phase angle are added geometrically and fed to the power system in each phase. Figure 4 shows the block diagram representation of EV load.

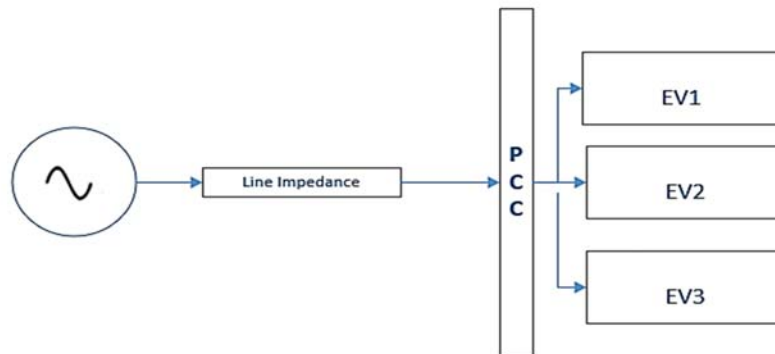


Figure 4: EVs connected to the grid

For the voltage source modeling, line impedance  $z = .001+j1e-6 \Omega$  is connected in the source side with  $2 \Omega$  internal resistance. The harmonic current is injected to the PCC using a controlled current source. A three-phase source is modeled with  $V_{rms} = 415 \text{ V}$  and the supply frequency =  $50 \text{ Hz}$ . The waveform of the load current is shown in Figure 5, showing that the load current is balanced. However, the waveforms are distorted due to the presence of harmonics. The THD due to this non-linearity is  $6.48\%$ , as shown in Figure 6.

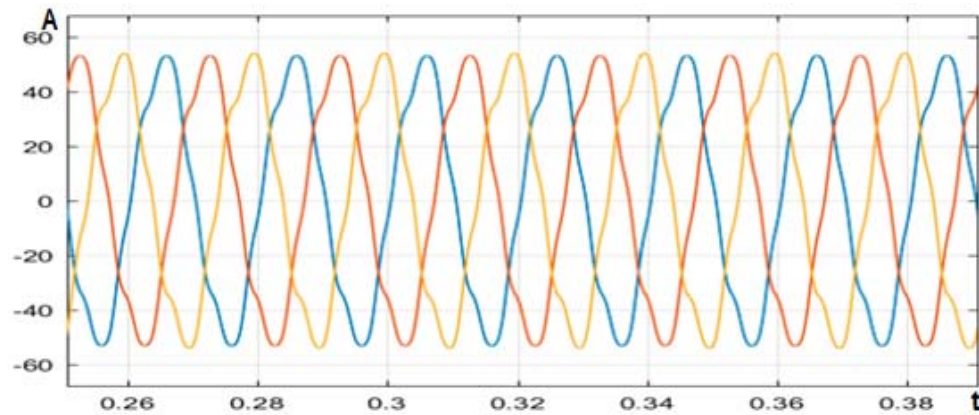


Figure 5: Current waveform of the non - linear load

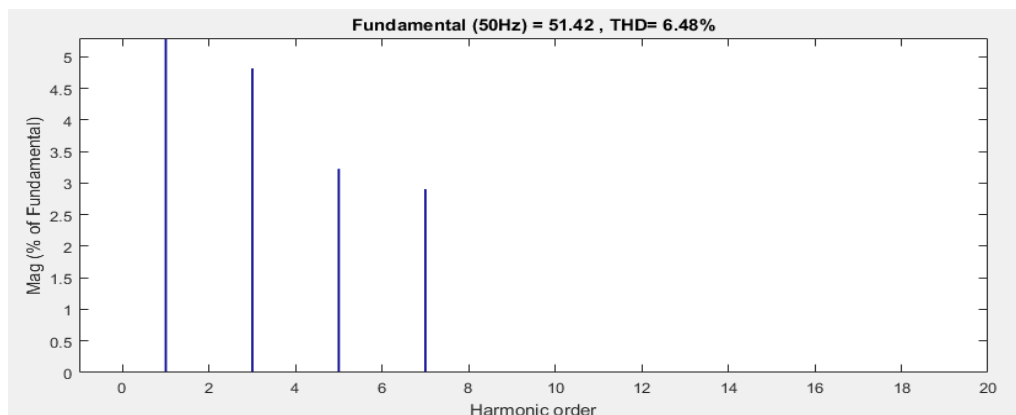


Figure 6: THD at source side due to a non-linear load

### **1.5 Harmonic mitigation methods**

The presence of harmonic content in the power system also increases due to an increased usage of non-linear load. It can cause poor power transfer to the load, thereby reducing the overall system efficiency. Many other issues also arise when the harmonic content available in the system exceeds the prescribed limit. The commonly used methods for harmonic mitigation are discussed in the following section (Kaiwart & Raju, 2016).

The methods for addressing the harmonic problems in the grid can be classified into two. The first method uses appropriate circuit topology, and the second method uses suitable filters. The commonly used circuit topologies to solve harmonic pollution in the power grid are as follows:

- ❖ Line Reactor
- ❖ K factor Transformer
- ❖ 12 and 18 pulses rectifier
- ❖ Phase shifting transformer

The advantages and disadvantages of these circuit topologies are explained in (Kaiwart & Raju, n.d.) and summarized in Table 4.

Table 4: Harmonic mitigation circuit topologies

	Advantage	Disadvantage
Line Reactor	Low cost. Moderate harmonic mitigation. Different percent impedance is available.	It causes a voltage drop. Cannot achieve THDi less than 35%
K factor transformer	It can handle heat associated with eddy current losses	Higher cost
12 and 18 pulse rectifier	12 pulse: 10 - 20% THDi-reduction 18Pulse: 5 – 10% THDi-reduction	THDi increases with decrease in load. If the load is unbalanced, then harmonic mitigation increases.
Phase shifting transformer	5 <sup>th</sup> and 7 <sup>th</sup> harmonic are canceled approximately for equal loading condition.	Additional impedance required to protect during short circuit condition.

The filtering techniques for harmonic mitigation can be further classified into the following:

- ❖ Passive filters
- ❖ Active filters
- ❖ Hybrid filters

### **1.5.1 Passive filters**

The idea behind passive filtering is to block harmonic currents flowing through the grid by either diverting them to a low impedance filter path, such as a parallel passive filter, or preventing them entirely via a high series impedance, such as a series passive filter. Passive filters are preferred to other harmonic mitigation methods due to their simplicity, low cost, and high efficiency.

One of the commonly used passive filters is a passive tuned filter. It provides a low impedance path that diverts the harmonic current to the filters rather than power lines. The tuning of passive elements is a major task in designing passive filters. If many harmonic currents should be filtered, then extensive system studies, engineering effort, and cost are required.

### **1.5.2 Active filters**

The working principle of an active filter is to precisely inject to the system voltage/current harmonics of nonlinear loads with the same magnitude and opposite sign to cancel each other and ensure clean waveforms in the power line. Active filters are smaller than passive filters.

These active filters are normally limited to several MW levels, and their cost increases under high power levels due to operating losses and large VA ratings. However, active filters are considered as the best method for harmonic mitigation because of their great filtering performance and solutions to various power quality problems, such as reactive power compensation for PFC, voltage regulation, and load balancing.

### **1.5.3 Hybrid filters**

Hybrid filters that combine passive and active filters in various configurations are introduced to reduce the initial cost and increase the efficiency of the filter structure. The basic principle of hybrid filtering is to improve the filtering capacity of a passive filter and to damp series and parallel resonances with a small rated active filter. However, the functionalities of hybrid filters are more limited than those of pure active filters, and their design involves higher engineering effort than passive filter design (Peng, 2001). Therefore, active filters are the best option for solving harmonic problems.

### **1.6 Active filter**

The harmonic pollution in the power system has increased gradually over the last two decades due to the increased usage of power electronic circuits. Thus, engineers should develop high-performance harmonic mitigation techniques to solve all power quality problems. The following three types of active filters are available depending on the function and type of non-linear loads: parallel type, series type, and a combination of both.

- Series active filter.
- Parallel (shunt) active filter.
- Combination of parallel and series active filter

#### **1.6.1 Series active filter**

The basic SAF configuration is shown in Figure 7. It is connected to a utility grid through a coupling transformer to isolate harmonic voltages. It is also used to regulate and balance the terminal voltage of non-linear loads.



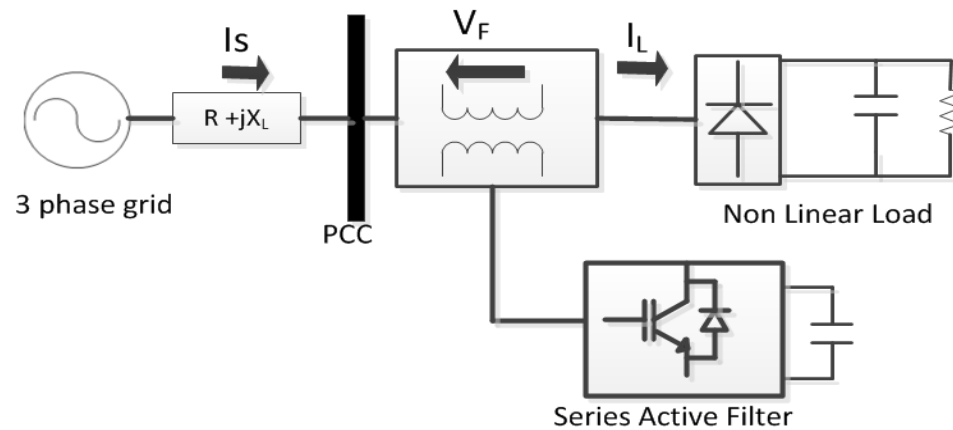


Figure 7: Series Active filter

A SAF reduces the voltage sag, swell, and flicker by injecting a voltage to the grid (Nikoomanesh, Alizadehe, Naderi, & Soltani, 2014). Generally, a SAF is employed when the nonlinear load acts as a harmonic voltage generator. A non-linear load is illustrated in this work as a general purpose diode rectifier with DC link and terminal loads.

### 1.6.2 Parallel (shunt) active filter (PAF)

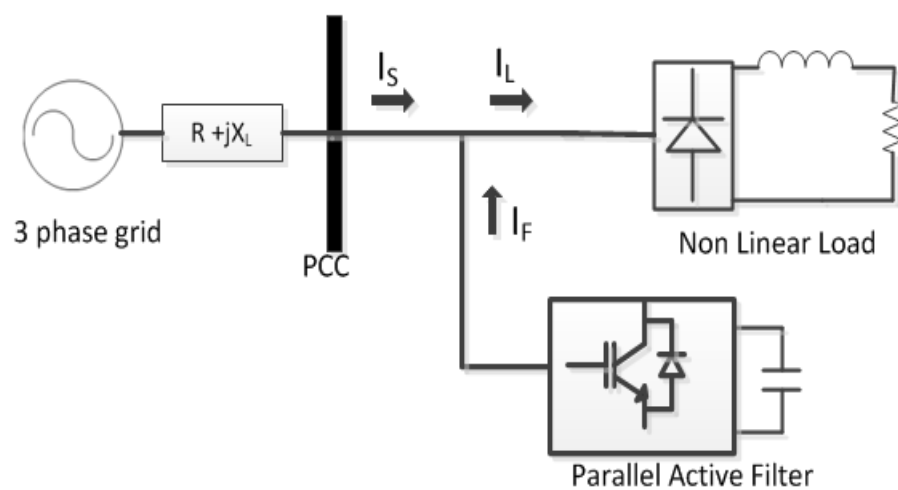


Figure 8: Parallel Active filter

A PAF is also called a shunt filter due to its parallel connection to the load. Figure 8 illustrates a PAF. In this configuration, the filter injects a compensating current into the system to cancel the harmonic current and to compensate for the reactive power current and the unbalanced current components on the AC side of a nonlinear load. If the PAF is connected to three-phase four-wire systems, then it is capable of compensating for the neutral current (zero sequence current) component. Therefore, using a PAF, the current drawn from the utility grid becomes free from harmonic content, balanced, and in phase with the utility voltage. A detailed description is provided in Chapter 2.

### **1.6.3 Combination of PAF and SAF**

The combination of SAF and PAF is called a unified power quality conditioner (UPQC), as shown in Figure 9. In this configuration, the SAF suppresses the voltage harmonics, sags, swells, and flickers and balances and regulates the load terminal voltages. The PAF compensates for the harmonics current, reactive power current, and unbalanced current components of a nonlinear load (Fujita & Akagi, 1998). The UPQC provides clean power. Hence, it can be used for critical and power quality sensitive loads, such as computers and medical equipment. The main disadvantages of the UPQC are its high cost and complex control.

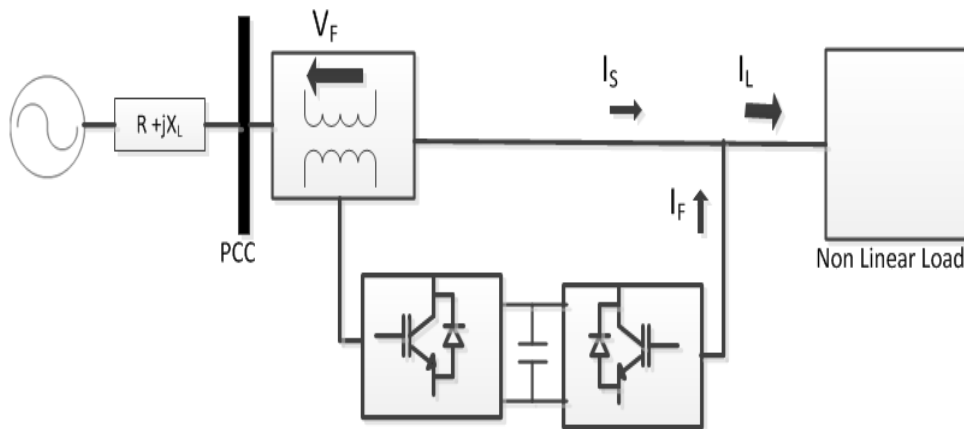


Figure 9: Combination of series and parallel active filter

### 1.7 PAF

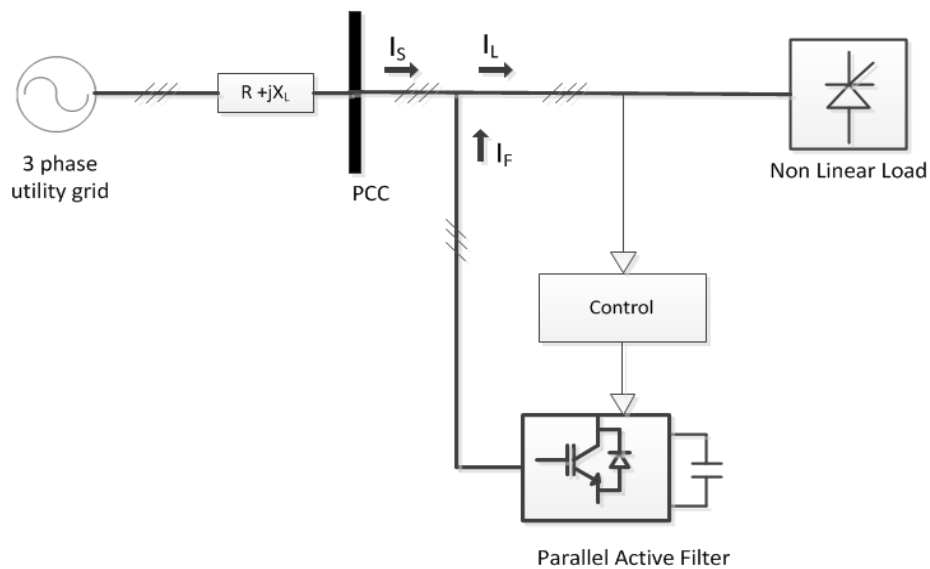


Figure 10: Block diagram of parallel active filter

Parallel Active Filter (PAF) is used to produce the compensating harmonic current. The current drawn from the grid is distorted due to the presence of harmonic loads connected to the grid. The control strategy of the PAF system determines the instantaneous load current and removes the harmonic content by injecting

compensating current, to nullify the load harmonic effect. This methodology facilitates the transformation of the current drawn from the grid as a purely sinusoidal waveform. Figure 10, illustrates the connection diagram of a three-phase non-linear load, connected to a three-phase three-wire supply.  $I_F$  is the compensating filter current injected to the grid whereas  $I_S$  is the source current.

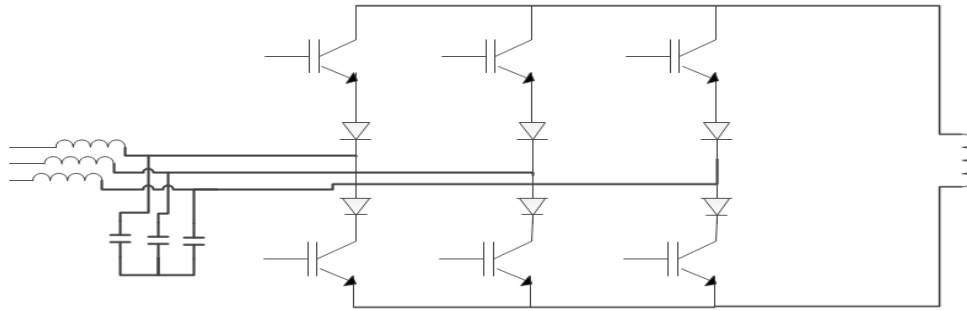


Figure 11: PWM current source inverter (CSI)

Two circuit topologies are commonly used to realize the PAF circuit requirement. Figure 11 depicts a PWM current source inverter (CSI). This model has insulated-gate bipolar transistors (IGBTs) with series-connected diodes for reverse blocking. These IGBTs have higher conduction and switching losses than IGBTs with anti-parallel diodes.

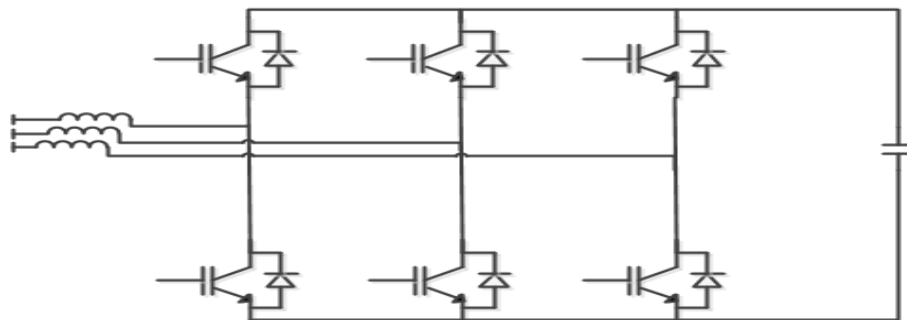


Figure 12: PWM voltage source inverter

Another circuit topology is the PWM VSI shown in Figure 12. In this configuration, the IGBTs have anti-parallel diodes. This circuit configuration is commonly available in the market because the DC link capacitors are low cost and are not as bulky as DC link inductors in CSIs. Moreover, the protection circuitry for CSIs is more complicated than that for VSIs. Therefore, VSIs are more efficient, more cost-effective, and smaller in size than CSIs (Routimo, Salo, & Tuusa, 2005).

### 1.7.1 Working principle of VSI

Inverters are devices that can produce an AC output waveform from a DC power supply. For sinusoidal AC outputs, the magnitude, frequency, and phase should be controllable. If a DC input is a voltage source, then the inverter is called a VSI. Figure 13 shows the function of a VSI. In this circuit, an AC load is connected across the DC link by using two single pole double throw (SPDT) switches. The main requirement of an inverter is to connect positive voltage ( $V_{dc}$ ), negative voltage ( $-V_{dc}$ ), and zero voltage to the load. Therefore, SPDTs should be utilized in both directions and block the DC bus supply when not in conduction. To satisfy this requirement, this study uses MOSFET with an anti-parallel diode.

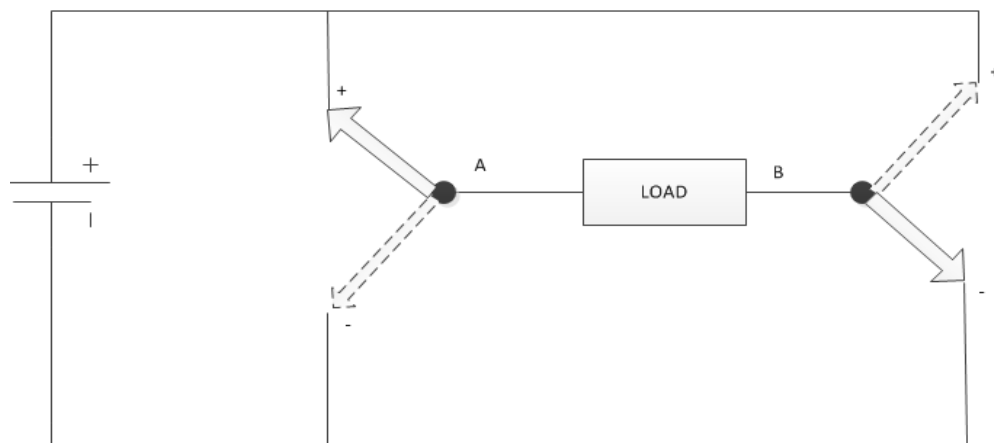


Figure 13: Single phase voltage source inverter

The realization of the circuit requirement is shown in Figure 14, which shows the use of MOSFET switches with anti-parallel diodes.



Figure 14: Single phase VSI circuit diagram

When the M1 transistor is conducting in a positive direction and the diode conducts in a negative direction, the M4 diode blocks the +Vdc voltage. To achieve this operation, the gate pulses for M1 and M4 and those for M2 and M3 should complement each other. All switching states and output voltages are listed in Table 5.

Table 5: Switching states and output voltage of single phase inverter

State	Switching state	Output voltage		
		$V_{A0}$	$V_{B0}$	$V_{AB}$
1	M1 and M3 are ON	$\frac{V_{dc}}{2}$	$-\frac{V_{dc}}{2}$	$V_{dc}$
2	M4 and M2 are ON	$-\frac{V_{dc}}{2}$	$\frac{V_{dc}}{2}$	$-V_{dc}$
3	M1 and M2 are ON	$\frac{V_{dc}}{2}$	$\frac{V_{dc}}{2}$	0
4	M4 and M3 are ON	$-\frac{V_{dc}}{2}$	$-\frac{V_{dc}}{2}$	0

### 1.7.2 Three-phase VSI

The power circuit diagram of a three-phase VSI is shown in Figure 15. In this circuit, six switches are connected in a particular manner. These switches are turned on and labeled as SW1, SW2, SW3, SW4, SW5, and SW6.

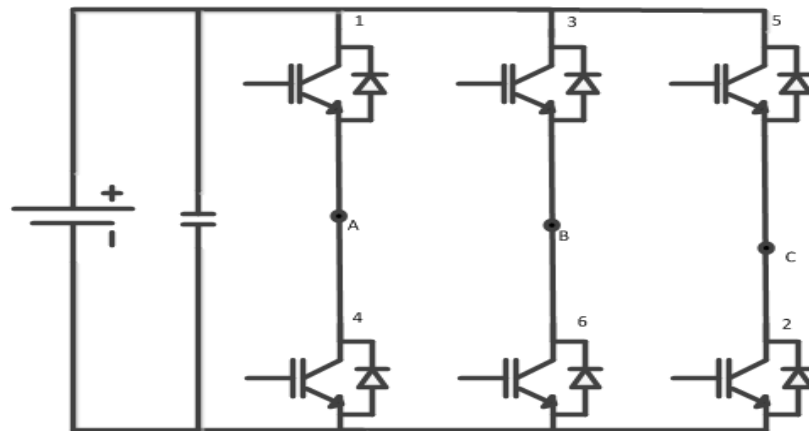


Figure 15: 3phase VSI

Figure 16 depicts the switching pattern of the three-phase VSI. In this configuration, each switch is turned on for  $180^\circ$  ( $\Pi$  radian). At any instance, three switches are in conduction mode, that is, either two switches from the upper group (connected to the positive terminal) and one switch from the bottom group (connected to the negative DC bus) or one switch from the upper group and two switches from the lower group. At any output cycle, six combinations of turned-on switches are available: (SW1, SW5, and SW6), (SW1, SW2, and SW6), (SW3, SW2, and SW1), (SW4, SW3, and SW2), (SW3, SW4, and SW5), and (SW6, SW5, and SW4). These combinations of switches conduct for a period of 60 degrees in the sequence to produce the output of three-phase waveforms.

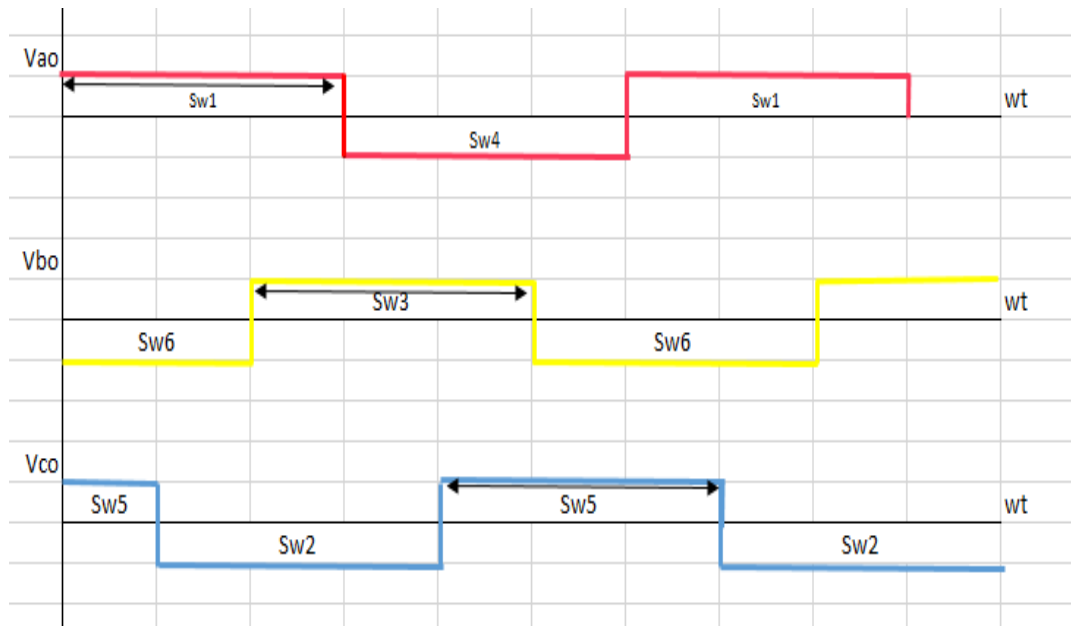


Figure 16: Switching patterns of 3-phase VSI

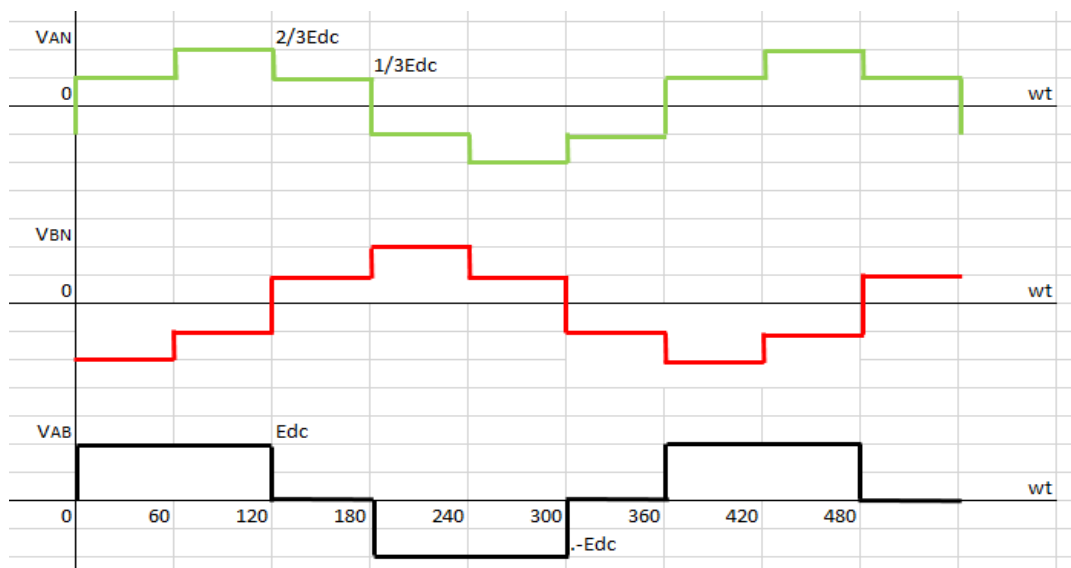


Figure 17: Phase and line voltage output of 3phase VSI

Relevant phase voltages are shown in Figure 17, presenting the output of the line voltage of AB. The figure shows that the phase voltages of  $V_{an}$  and  $V_{bn}$  are



exactly  $120^\circ$  apart. The maximum output voltage at any instance is two-thirds of the DC link voltage.

### 1.8 Power factor correction (PFC) converters

Modern EV chargers are equipped with PFC converters for power factor improvement. The power quality at AC mains can be improved using PFC converters. Single-phase AC–DC PFC converters with high-frequency isolation comprehensively were studied by Singh, Singh, Chandra, & Al-Haddad (2011). The input and output voltages are classified as buck, boost, and buck–boost topologies. Buck and boost converters are further classified into forward, push–pull, half bridge, and full bridge with HF transformer isolation. The buck–boost type converter is subcategorized into flyback, Cuk, Sepic, and Zeta converters with MOSFETs with high-frequency isolation. These classifications are shown in Figure 18.

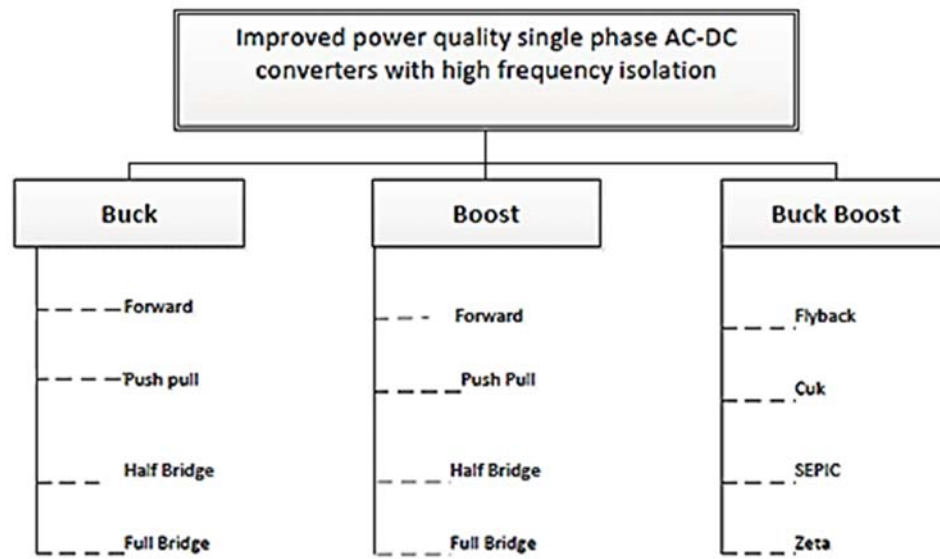


Figure 18: Power factor correction with HF isolation

### 1.8.1 Comparison of PFC converter topologies

The cost of a PFC converter controller increases with the power rating, and such effect equates to an increase of passive and active components. Flyback and zeta (single switch topologies) converter configurations are preferred over Zeta and Sepic converters because of their additional protection against overcurrent and inrush current. In addition, Cuk converters require a small cores, which reduce core and copper loss. Moreover, flyback converters require only a capacitor as an output filter. Push-pull and half bridge (two switches) configurations use one switch at a time, leading to equal switching losses in comparison with those for a single switch converter. However, with the cost of additional switches and circuitry, they can be used for high power applications.

In hardware implementation, many configurations are used to improve the power factor to 0.99 (Routimo et al., 2005, Lee et al., 2011). Some of the research findings include line and load regulations depending on the gain of the PFC controller and the turn ratio of the HF transformer. The control and protection circuits configuration are the major factors in electromagnetic interference and noise suppression. In addition to PFC, many other parameters, such as voltage ripple, transient response, device rating, and cost of the circuit, are involved in the selection of converter topologies for particular applications.

Although EV chargers are designed to satisfy all power quality standards, they have evident harmonic injections to the grid in actual practice (Aljanad & Mohamed, 2016), (Aiqiang Pan et al., 2016). Hence, an active filter is modeled with normal PI and fuzzy PI controllers to mitigate the THDs generated by EV chargers. An issue with normal PI controllers in active filters is that the voltage regulation of the DC link is

slow to reach its reference value. This performance can be improved by replacing the normal PI in the DC link control with a fuzzy logic controller (FLC).

The utility grid will produce only the fundamental current for the EV charger and remaining harmonic as well as Reactive component of the charger is supplied from the VSI by controlling the switching pulses of MOSFETs. This operation mode helps to make the grid current to become pure sinusoidal wave. So one of the biggest challenge is to identify the accurate reference current to compensate the harmonics and reactive component. Various techniques already available that are capable of generating accurate reference current, they are explained in the next section.

## 1.9 Control strategies for shunt active filter

### 1.9.1 Constant instantaneous power technique

In this technique Clarke transformation is used to transform ABC to alpha beta values. And inverse Clarke's transformation is used to convert the alpha beta values to ABC three phase axis values. Instantaneous power before and after the transformation remains same, hence these matrices are power invariant matrix. Instantaneous power on alpha beta axis is given by the Equation 1.4.

$$S = (V_{\alpha}I_{\alpha} + V_{\beta}I_{\beta}) + (V_{\beta}I_{\alpha} - V_{\alpha}I_{\beta}) \quad (1.4)$$

Reference current can be calculated by the equation 1.5

$$\begin{bmatrix} i_{c\alpha}^* \\ i_{c\beta}^* \end{bmatrix} = \frac{1}{v_{\alpha}^2 + v_{\beta}^2} \begin{bmatrix} V_{\alpha} & V_{\beta} \\ V_{\beta} & -V_{\alpha} \end{bmatrix} \begin{bmatrix} -\tilde{p} + \bar{p} \text{ loss} \\ -q \end{bmatrix} \quad (1.5)$$

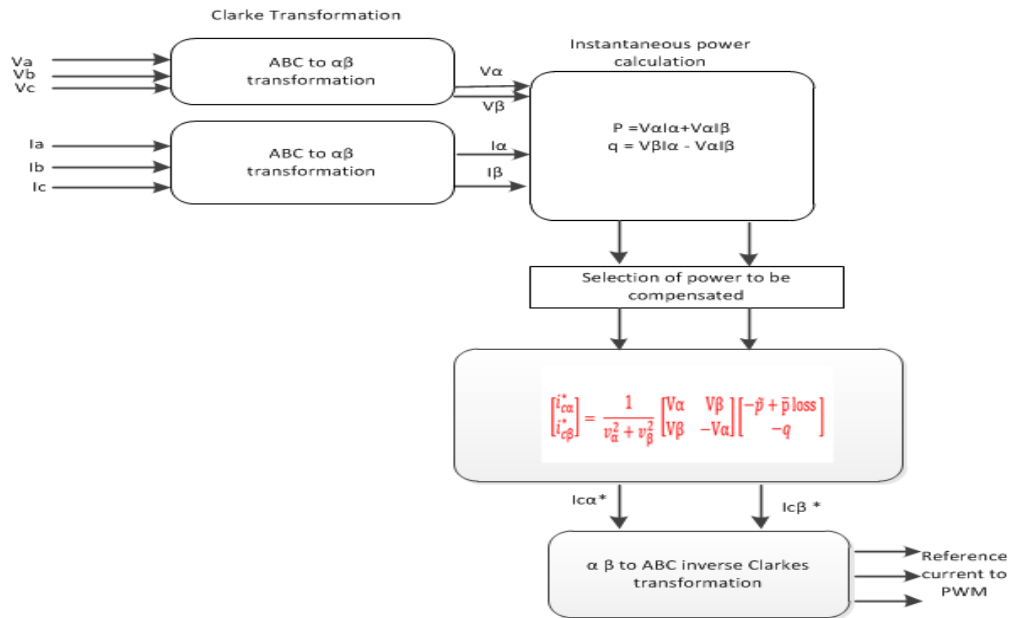


Figure 19: Block diagram of constant instantaneous power method

Here, Instantaneous active power  $P = V_{\alpha}I_{\alpha} + V_{\beta}I_{\beta}$  and whereas Instantaneous reactive power  $q = V_{\beta}I_{\alpha} - V_{\alpha}I_{\beta}$ . Now this Active part is separated to average part  $\bar{p}$ ,  $\tilde{q}$  and oscillating part  $\tilde{p}$  &  $\tilde{q}$  by using second order Butterworth low pass filter with cut off frequency 50 Hz. In this technique  $\tilde{p}$  and the entire Instantaneous reactive power  $q$  ( $\tilde{q} + \bar{q}$ ) is utilized to calculate the reference current. Inverse Clarke's transformation is used to convert this reference current into ABC frame as shown in Figure 19. This method is applicable only in the balanced case. In unbalanced case this will give bad result.

### 1.9.2 Generalized fryze currents minimization technique

One of the biggest advantages of this method is that it does not require Clarke's transformation to find the reference current. In this method, it directly calculates the instantaneous voltage and current for each phase. Generalized Fryze current is given by Equation 1.6. The block diagram is shown in Figure 20.

$$i_{wk} = G_e V_k \quad k = (a, b, c) \quad (1.6)$$

$G_e$  = Equivalent conductance

$$G_e = \frac{1}{T} \int_0^T \left( \frac{v_a i_a + v_b i_b + v_c i_c}{v_a^2 + v_b^2 + v_c^2} \right) dt \quad (1.7)$$

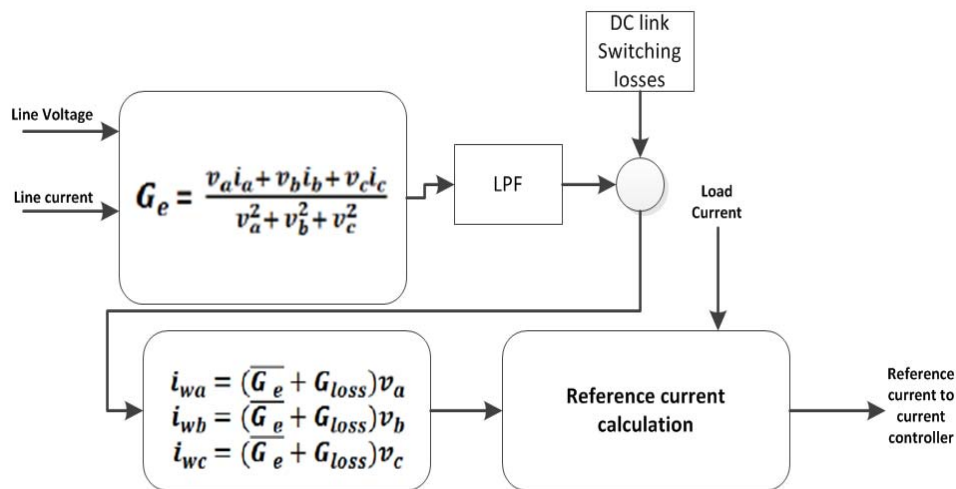


Figure 20: Fryze current control block diagram

This current and current related to the switching losses of VSI is also added. This reference current fed to the PWM block to generate the gate pulses. Fryze current method draws less RMS current than previous method but it has higher THD in the source current.

### 1.9.3 Synchronous reference frame controller (SRFC)

This method involves ABC to dq frame and vice versa transformation to find the reference current. This method is useful when there is a distortion and / or unbalance from supply side. A detailed explanation of this method is given in the Chapter 2.

### 1.10 Fuzzy logic controller (FLC)

The concept of the FLC was first presented by Professor Zadeh Lotfi in 1965. He proposed a method for solving a process involving imprecise data with complex inputs. The FLC is simple to use in designing the control system of a process because it does not require an exact mathematical model of the plant or process. Researchers (Usman, Hizam, & Mohd Radzi, 2013. Colak, Bayindir, Kaplan, & Tas, 2010) used FLCs in active filters. Fuzzy logic uses membership function (MF), and its value ranges between 0 and 1. Figure 21 shows the block diagram of a fuzzy controller.

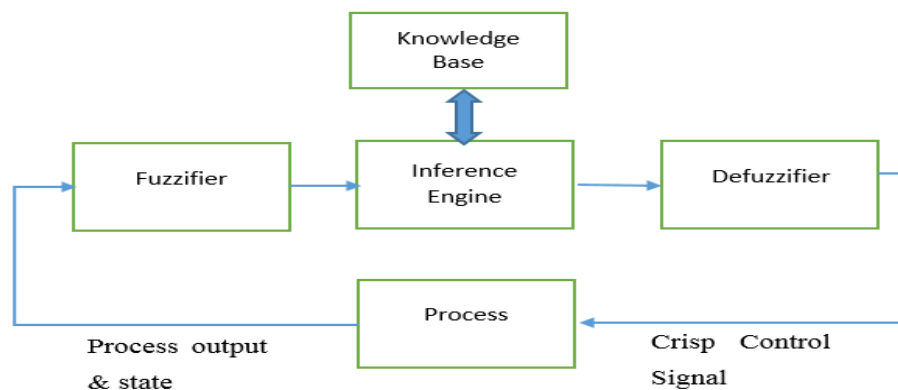


Figure 21: Block diagram of fuzzy logic controller

#### 1.10.1 Fuzzification

It helps to convert crisp numbers into fuzzy sets. The fuzzification involves expressing the system inputs and outputs in linguistic terms so that it can be easily applied to a complex system. In this process, the system input decomposes into one or more fuzzy sets. Triangular membership function (MF) is used in this study because it is easy to represent. The degree of MF of any input can be easily interpreted from fuzzy sets.

### **1.10.2 Knowledgebase**

In fuzzy logic systems, the fuzzy knowledge base represents the facts of the rules and linguistic variables based on the fuzzy set theory so that the knowledge base systems will allow approximate reasoning.

### **1.10.3 Fuzzy inference engine**

In this process mapping the input vector to output vector using fuzzy logic. The mapping carried out based on some set rules on the fuzzy sets, i.e membership function, if-then rules, and fuzzy logic operator. Mamadani and Sugeno type are the main types of fuzzy inference systems. In the current study Mamdani type fuzzy inference system is used. It involves fuzzify the input, apply fuzzy operator, apply implication method, apply aggregation method and finally defuzzification.

### **1.10.4 De-Fuzzification**

In this process transfer fuzzy inference engine's results into a crisp output. Decision-making algorithm to select best crisp value based on the fuzzy set. Commonly used defuzzification methods are center of gravity (COG), center average method and mean of maximum (MOM). COG method is used in this thesis. This method returns value of the center of the area under the curve.

The inputs to the FLC are errors and changes of errors between the DC link voltage and a reference voltage. The output from the FLC includes proportional gain ( $K_p$ ) and integral gain ( $K_i$ ). The P and I values are calculated using fuzzy control techniques to regulate the DC link voltage. A detailed explanation of input MF, output MF, and Mamdani's technique is presented in Chapter 2.

### 1.11 Problem Statement

The major concerns of electric car owners are mileage and the time required to recharge batteries. However, due to the tremendous technological development in EV technology, the mileage of EVs has increase, and the time required to recharge the battery packs of EVs is significantly reduced. Many off-board chargers are available, and the number of EV charging stations is expected to increase in charging networks. These off-board high-speed chargers significantly reduce EVs' charging times (Yilmaz & Krein, 2012). However, during the charging process, the EV charger load injects harmonics to the grid (Guo et al., 2018; Aiqiang Pan et al., 2016; Ul-Haq, Perwaiz, Azhar & Ullah Awan, 2018). The power demand of an EV is dependent upon the state of charge (SOC) of the battery. Hence, power consumption varies from zero SOC to full SOC. During charging process harmonics injected to the grid due to the power electronic converter in the EV charger.

EV charging station loads comprise EV loads and non-EV loads. During the charging period, these loads inject harmonic currents to the grid. If this harmonic content injected to the grid exceeds the limits set by the standards, then it should be controlled; otherwise, it will lead to the overheating of cables, overloading of transformers, and poor power transfer. Ultimately, the overall system efficiency is reduced. Although these chargers are designed to satisfy all power quality standards, such as IEEE 519-1992, SAE-J2894, IEC1000-3-2, and (NEC) 690, they often seem to inject more harmonic currents to the grid due to many circumstances.

An EV charger should maintain an acceptable power quality waveform at the PCC. These standards limit the allowable harmonic and DC current injection into the grid; thus, modeling an EV charger is expected to help determine the rates of harmonic



distortions. A charger model with a filter is developed in MATLAB/Simulink software. The charger is modeled as an injected current harmonic source, and the filter is used as a VSI. Neutral current compensation is also achieved by using two IGBTs, This helped to inject required compensating current to the neutral conductor during any unbalanced loading. The fuzzy logic controller is used for self-tuning the PI controller used in the DC link voltage control. The circuit diagram and simulation results in various operating conditions are explained in Chapters 2 and 3, respectively.

### **1.12 Objective**

- To model an active filter to mitigate the harmonics generated by EV chargers.
- To analyze the performance of the filter in various operating conditions.

### **1.13 Scope of the work**

- A charger model is developed to determine the THD generated by an EV charger. A harmonic current profile from a commercially available EV is used to model the charger. The power rating of the charger, voltage distortion and power factor improvement, and state of charge of the battery pack are excluded from the scope.
- The performance of the VSI is compared with that of a conventional and fuzzy PI.

## **Chapter 2: Development of Active Filter for Harmonic Elimination**

### **2.1 Proposed EV charger model**

Power electronic converters are used for conversion from AC to DC supply, which is required to charge EV batteries. The power delivered to the battery varies continuously from low to full SOC. Therefore, the charging current varies throughout the charging period. Given the power of EV chargers and the features of EV charging loads, a detailed study is necessary to ensure that the power grid network standards are still satisfied even when many EVs are charged simultaneously. EV battery chargers draw a distorted current from the utility because the diode rectifier in the EV charger draws non-sinusoidal current from the grid, thereby increasing the THD of the current waveform. If the injected current's THD is greater than the allowable limit, then it needs to be controlled.

Currently, EV chargers exhibit features that support the power grid, such as current waveform shaping and PFC techniques. The effect of the simultaneous charging of EVs on THDi is studied. The harmonic current profile of a commercially available EV is used to model the charger. In this model, the dominant harmonic currents and their phase angle values from the EV harmonic spectrum are used.

For the analysis purpose, Harmonic currents of a Fast charger is considered in this study. Both magnitude and phase angle values are used to model the harmonic current source. Figure 22 represents the block diagram of the connection of an EV charger to the power system grid. Three similar EV chargers are plugged into the power grid on each phase respectively. The amplitude and phase angle values of the fundamental, third, fifth, and seventh harmonic currents are injected into the power

grid using a controlled current source block in MATLAB/Simulink. This block generates a current on the basis of the input signal of the block.

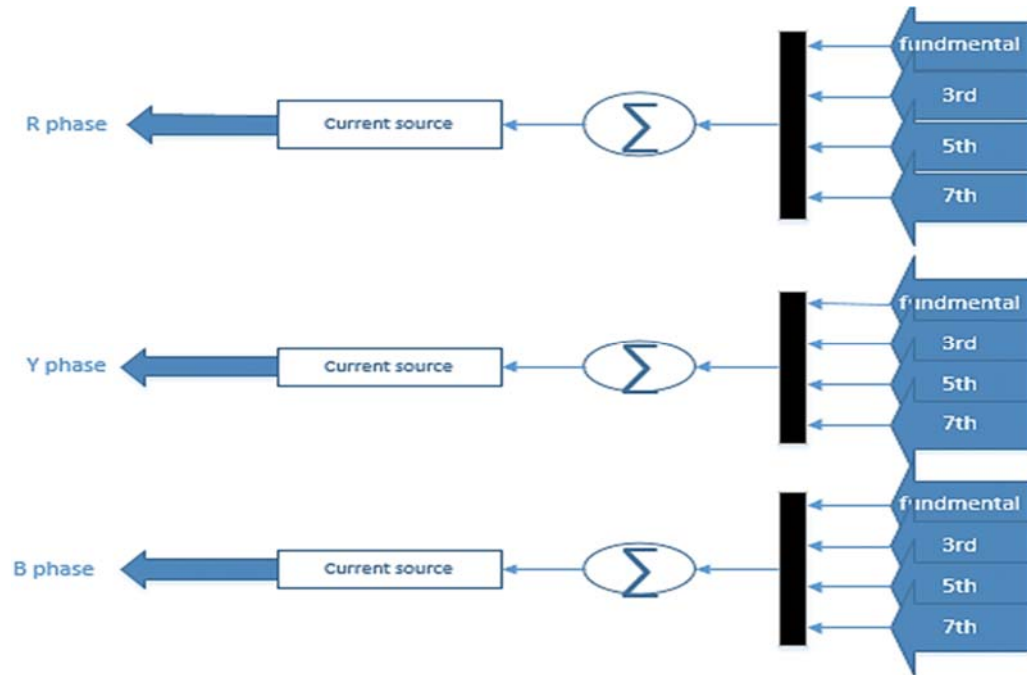


Figure 22: EV harmonic model

The harmonic current profile of the Nissan Leaf charger is used to model the EV charger (Aiqiang Pan et al., 2016). Table 6 shows both the magnitude and phase angle of different harmonic orders.

Table 6: Line current harmonic content of an EV charger

Harmonic order	Magnitude (%)	Angle (deg)
1.00	100.00	-26.00
3.00	25.00	-94.00
5.00	17.00	-96.00
7.00	14.20	-72.00
9.00	9.69	-68.00
11.00	5.04	-49.00
13.00	1.80	-49.00
15.00	0.37	-46.00

Each harmonic current is added geometrically and injected to the power grid using the Mux and summation block in Simulink.

The harmonic current in the R-phase is injected in exactly the same manner. However, in the Y and B phases, these currents are injected  $-120$  degrees and  $-240$  degrees, respectively, to obtain a balanced waveform. Figure 23 shows the waveform of the three-phase line current. The figure shows that the current in each phase is balanced. Figure 24 represents the circuit diagram model of the EV charger plugged into each phase.

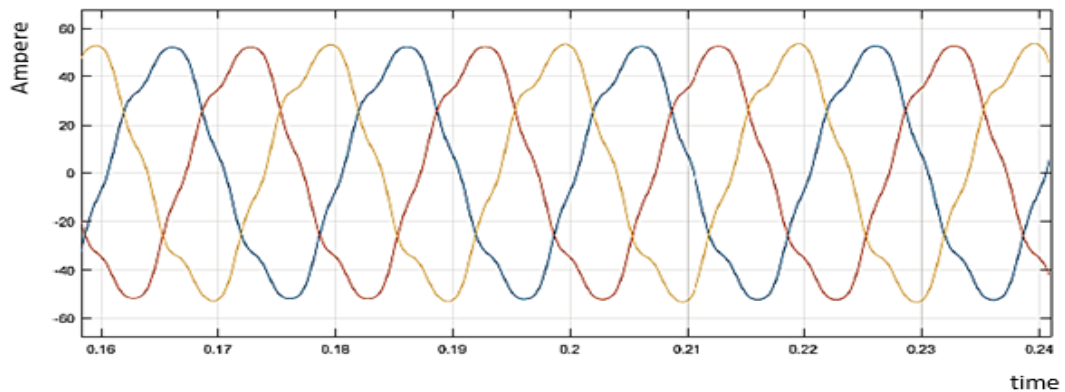


Figure 23: Three phase load current of an EV charger

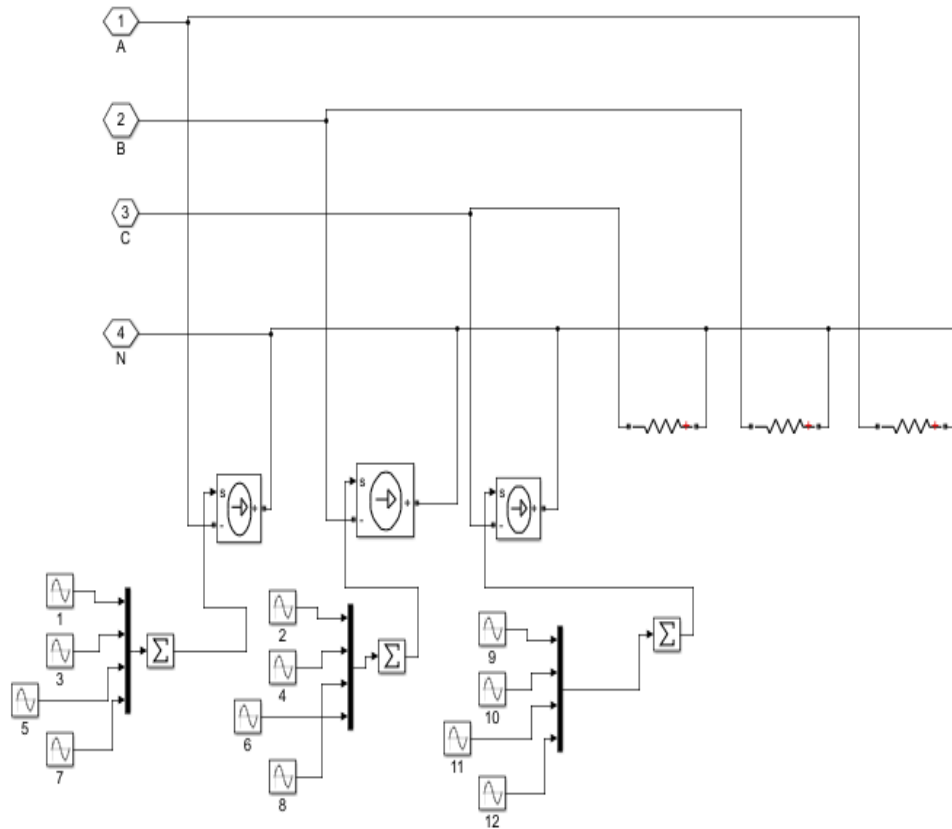


Figure 24: Circuit diagram model of an EV charger

For the sake of simplicity, among the harmonic current spectra, only the following dominant currents are used: third, fifth, and seventh harmonic currents. Similarly, all other harmonic currents can be injected to the grid to analyze the total harmonic current distortion. For the simulation, the grid and line parameters listed in Table 7 are selected.

Table 7: Grid modeling parameters

	Parameter	Value
AC Grid	Line Voltage (Vs)	415 V
	Frequency(fe)	50 Hz
	Line inductance(Ls)	100 $\mu$ H
	Line Resistance	0.01 $\Omega$
	Source resistance (Rs)	2 $\Omega$
	Sample Time	1 $\mu$ S

In calculating the THDi, the fundamental load current ( $I_{L1}$ ) and short circuit current ( $I_{sc}$ ) should be determined. The fundamental load current can be calculated from computer simulation, whereas the short circuit current can be calculated using the following formula:

$$I_{sc} = \frac{V_s}{\sqrt{3} * \sqrt{R_T^2 + X_T^2}} \quad (2.1)$$

Where,  $R_T$  = Total resistance of the system (Source resistance+ line resistance).

$X_T$ =Total inductive reactance of the system (internal reactance of the source + line reactance).

After substituting all the listed values in Table 7 in Equation 2.1,  $I_{sc}$  is found to be 119.2 A, and the fundamental component of the load current is 36.36 A. By plugging the calculated value on  $I_{sc}/I_{L1}$  is found to be 3.27. As per IEEE 519-1992, the THD allowed for this range is 4. Figure 25 shows that the THD current is 6.48%, which

exceeds the limit set by the IEEE Std. 519-1992. Therefore, the EVs plugged into the grid injects harmonics that exceed the allowable limit. Thus, a PAF is used to mitigate these harmonics and thereby obtain a less harmful harmonic injection from the charging station. Fast Fourier transform (FFT) analysis method in MATLAB/Simulink is used to determine the THD generated by these EV chargers. The screengrab of the FFT analysis results from MATLAB/Simulink is shown in the following section.

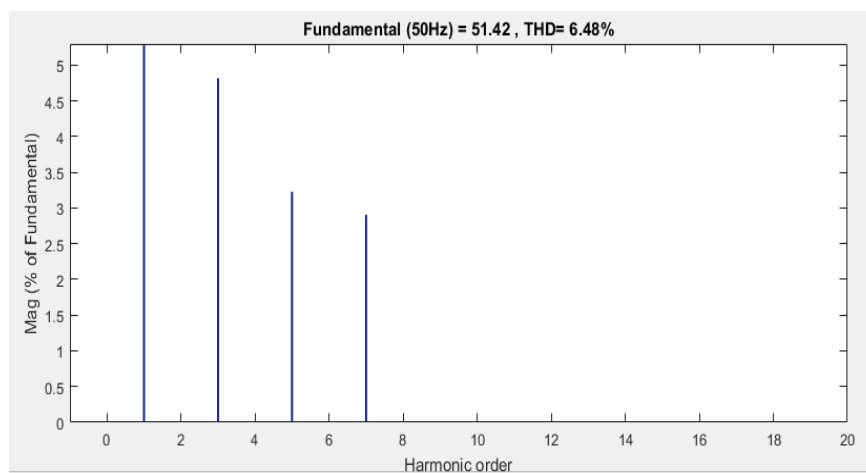


Figure 25: THD at the source side

## 2.2 Features of the parallel active filter

### 2.2.1 Harmonic producing nonlinear loads

Nonlinear loads can be classified into two. The first is the harmonic current source-type nonlinear load, and the second is harmonic voltage source-type nonlinear load. The harmonic current source type is a three-phase thyristor rectifier with a DC side inductance and a resistor. In this configuration, due to the sufficient inductance value at its DC side, it produces a nearly constant DC current. The harmonic current content of the rectifier's input current (load current) is not greatly dependent on the AC side. Therefore, this type is considered a harmonic current source-type nonlinear

load. However, a diode rectifier with a sufficient smoothing DC capacitor is considered harmonic voltage source-type nonlinear loads because the voltage at the input terminals of the rectifier is less dependent on the AC side.

The EV charger is modeled as the source of injected current harmonics. A detailed study of the harmonic current source-type nonlinear load is conducted. The per-phase equivalent circuit of a harmonic current source-type nonlinear load can be represented as Norton's equivalent circuit, as shown in Figure 26.

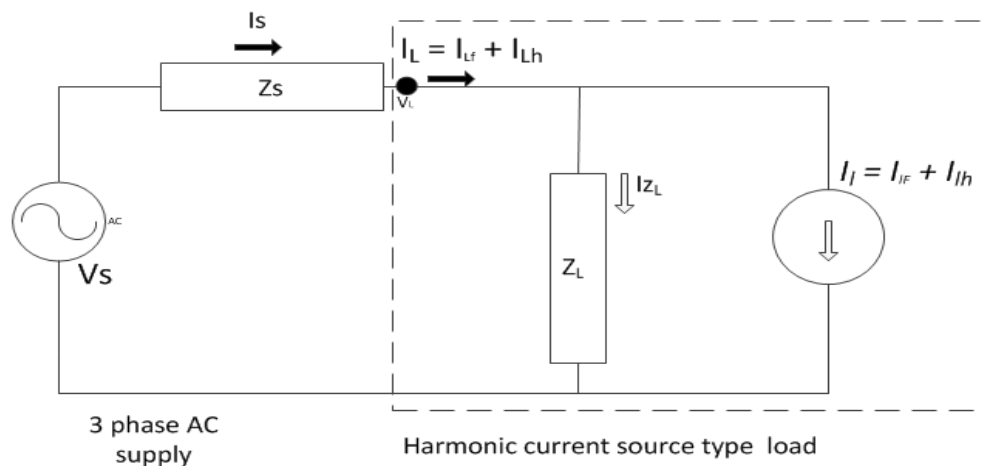


Figure 26: Norton equivalent harmonic current source

where the three-phase AC supply is represented as a voltage source with source voltage ( $V_s$ ) and  $Z_s$  is the source impedance.  $I_I$  is the current source, and the parallel impedance  $Z_L$  represents the equivalent current source.  $I_L$  is the total current drawn by the load.



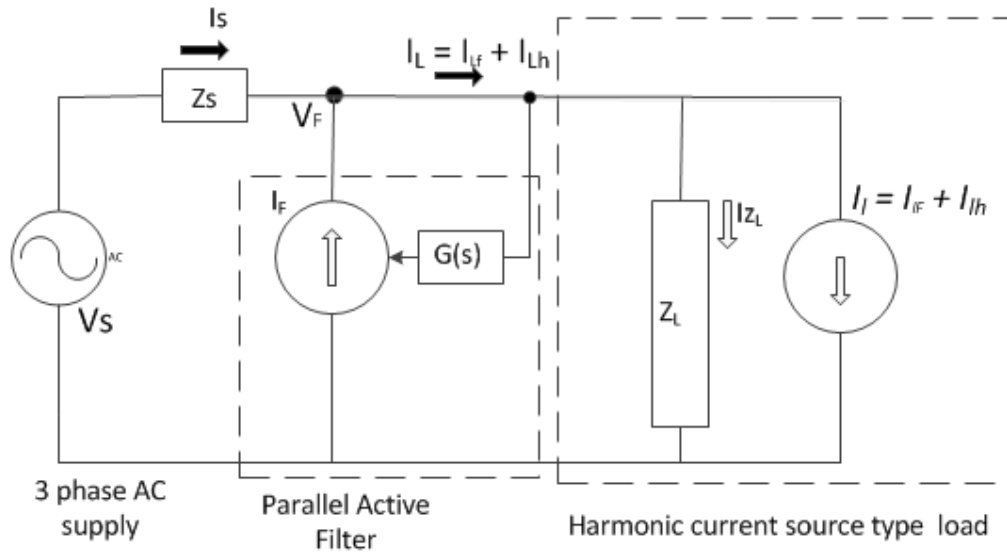


Figure 27: Norton equivalent circuit with PAF

The PAF is modeled as a harmonic current generator to compensate for the load current harmonics. Thus, the PAF in Figure 27 is represented as a current source of  $I_f$ . The filter current is defined by the following equation:

$$I_f = G(s) \times I_L \quad (2.2)$$

where  $G(s)$  is the transfer function of the PAF. The following equation is derived by analyzing the circuit:

$$I_s = \frac{Z_L}{Z_s + \frac{Z_L}{1-G(s)}} I_l + \frac{1}{Z_s + \frac{Z_L}{1-G(s)}} V_s \quad (2.3)$$

$$I_L = \frac{\frac{Z_L}{1-G(s)}}{Z_s + \frac{Z_L}{1-G(s)}} I_l + \frac{1}{(1-G(s)) \left[ Z_s + \frac{Z_L}{1-G(s)} \right]} V_s \quad (2.4)$$

The transfer function  $G(s)$  of an ideal PAF is zero at the fundamental frequency and approximately equal to unity at all harmonic frequencies,  $|G(s)|_h = 1$ . If the

condition given by  $(Z_L/|1-G(s)|_h) \gg |Z_s|_h$  is satisfied for the harmonic frequencies, then Equation 2.3 and 2.4 can be respectively written as follows:

$$I_F \cong I_{LH} \quad (2.5)$$

$$I_{sh} \cong (1 - G(s)) I_{lh} + \frac{1-G(s)}{Z_L} V_{sh} \quad (2.6)$$

Equation 2.5 indicates that the active filter current is approximately equal to the load harmonic currents and that the line current becomes harmonic-free due to  $|1-G(s)|_h \approx 1$  if the condition  $(Z_L/|1-G(s)|_h) \gg |Z_s|_h$  is satisfied. Hence, this condition must satisfy the PAF to compensate for the load current harmonics and to provide sinusoidal line currents.

$$I_{Lh} \cong I_{lh} + \frac{1}{Z_L} V_{sh} \quad (2.7)$$

Equation 2.7 implies that the active filter current does not flow through  $Z_L$ . To satisfy this condition, the load impedance should be larger than the source impedance and  $|1-G(s)|_h \ll 1$ .

Equation 2.3 can be rewritten as (2.8) using the above condition as follows:

$$\frac{I_s}{I_l} = 1 - G(s) \quad (2.8)$$

$$|1-G(s)|_h \ll 1. \quad (2.9)$$

Equation 2.9 shows that if the condition  $|Z_L| \gg |Z_s|$  is satisfied, then the PAF's performance depends on the transfer function only and not on supply impedance.

### 2.3 Voltage source inverter connected to EV charger

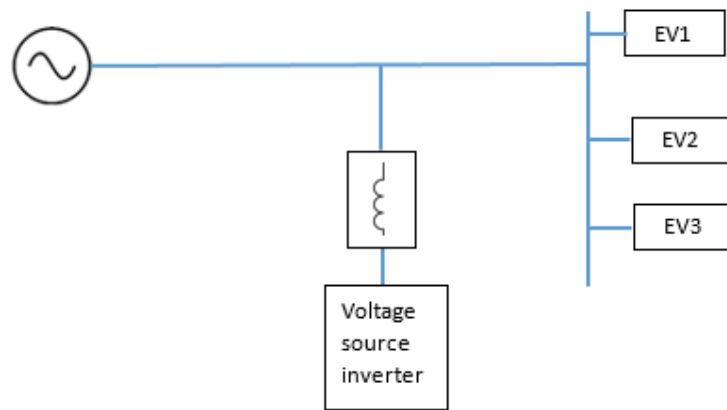


Figure 28: EVs with VSI

Figure 28 shows that three EVs are connected to the grid. The VSI is used to mitigate the harmonics injected by the EV chargers. The harmonic content in a power system network should be maintained at less than the limits set by the IEEE to reduce the negative effects of harmonic currents. The finding shows that the THD injected to the grid exceeds the allowable limit. Thus, some methods to mitigate the harmonics should be introduced. An active filter is used to mitigate THD. In this system, the VSI is used as an active filter, the fundamental harmonic current is filtered, and the phase and amplitude of the remaining current are analyzed. Once the filter understands the harmonic current, the filter injects inverse current to the power system to cancel all the harmonic currents. Moreover, the neutral current compensation is carried out in a similar approach.

In carrying out the above task, bi-directional semiconductor switches are used in the Simulink model. Additional circuitry and controls are required to produce gate signals. These gate signals are used to control the phase and neutral semiconductor switches. A detailed block diagram is shown in the following section.

## 2.4 Filter control

### 2.4.1 Phase locked loop (PLL)

PLL is used in this system to obtain the phase of the input signal. The grid is modeled as a voltage source, and the current to the voltage is controlled; hence, voltage PLL is used. The input voltage from the load side measurement block is fed to the PLL through the gain to obtain the phase of the voltage. This phase angle is required for ABC to DQ transformation. Figure 29 shows the block diagram of the PLL.

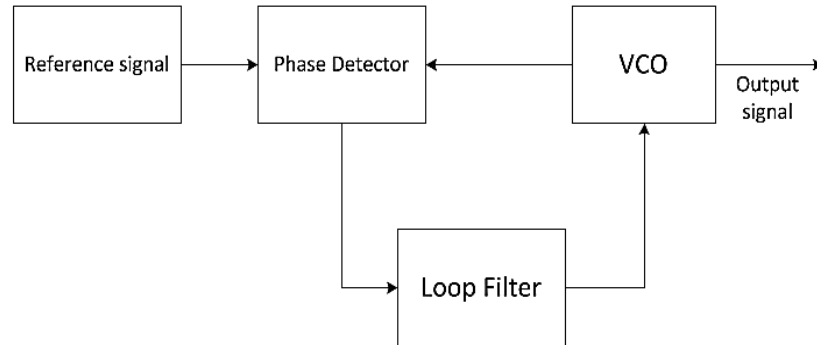


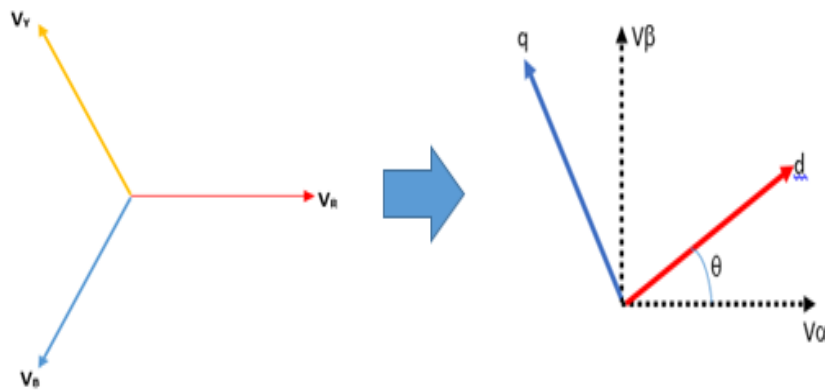
Figure 29: PLL block diagram

The reference signal is the voltage from the load side measurement block, which is compared with the voltage from the VCO connected to the phase detector. The phase of both signals were compared, and an error voltage is produced. This error signal corresponds to the phase difference between the two signals. The loop filter is used to remove any high-frequency elements on the signal. This process continues until the error cannot be reduced any further, indicating that the phase difference between the two signals is reduced along with their frequencies.

### 2.4.2 ABC to dq0 transform

The ABC to dq0 transformation block in Simulink is used to convert the three-phase ABC current waveform into direct, quadrature, and zero axis components. The block requires the phase of the input signal. Thus, the PLL output and current signal are connected. After the conversion, Demux is used to separate the block output into d, q, and 0 axis components. An active power component is obtained from the d axis, a reactive power component is obtained from the q axis, and a zero sequence current is obtained in the 0 axis. A detailed control strategy of the circuit configuration is explained in the following sections.

#### ABC to DQ transform



$$V\alpha = V_a - V_c \cos 60 - V_b \cos 60 \quad (2.10)$$

$$V\beta = V_b \cos 30 - V_c \cos 30 \quad (2.11)$$

$$\begin{bmatrix} V\alpha \\ V\beta \end{bmatrix} = \begin{bmatrix} 1 & -\cos 60 & -\cos 60 \\ 0 & \cos 30 & -\cos 30 \end{bmatrix} \begin{bmatrix} V_a \\ V_b \\ V_c \end{bmatrix} \quad (2.12)$$

$$\begin{bmatrix} Vd \\ Vq \end{bmatrix} = \begin{bmatrix} \cos\theta & \sin\theta \\ -\sin\theta & \cos\theta \end{bmatrix} \begin{bmatrix} V\alpha \\ V\beta \end{bmatrix} \quad (2.13)$$

### 2.5 Synchronous reference frame controller (SRFC)

The basic working principle of the SRFC was established in [24]. The SRFC is used to calculate the reference current. In this method, the three-phase load current ABC is transformed into two axes, namely, d–q frame. The q axis leads the d axis by 90°. This reference frame rotates at the same speed as the system frequency. Figure 30 shows that the phasor rotates at speed “w”. Thus, the d–q frame rotates with the same speed as “w”.

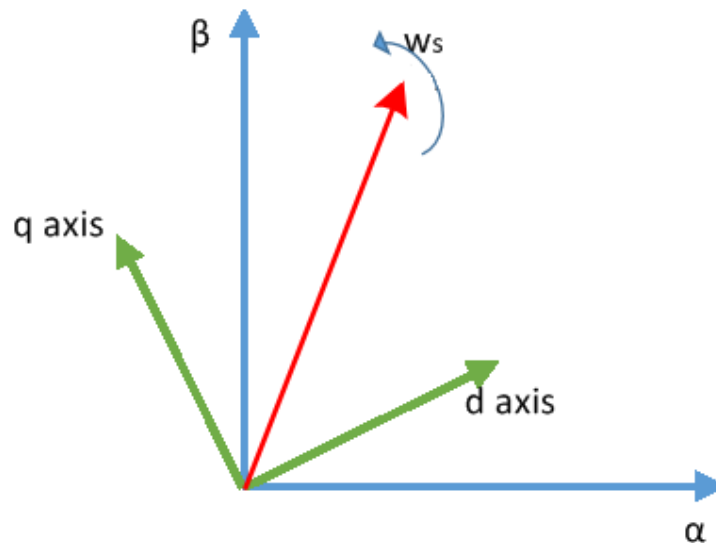


Figure 30: ABC to DQ transformation

Therefore, the relative speed between the d–q frame and the reference vector is zero. Hence, we observe a fundamental current as a DC quantity and all other harmonic currents as AC quantities. We can easily identify the DC and AC quantities by using appropriate filtering methods. Then, DQ to ABC transformation is used to obtain the three-phase reference current.

### 2.5.1 VSI with positive sequence SRFC

The main purpose of a VSI is to convert DC power back to AC power with the required frequency and voltage. Figure 31 shows that the MOSFET with the anti-parallel diode is used as a switching device. These switches turn on and off at regular intervals to provide the rectangular pulse of voltage to each phase. A bi-directional rectifier is selected because it can transfer power from the source to the load side and vice versa. Thus, the rectifier works in two modes, namely, rectifier mode and inverter mode.

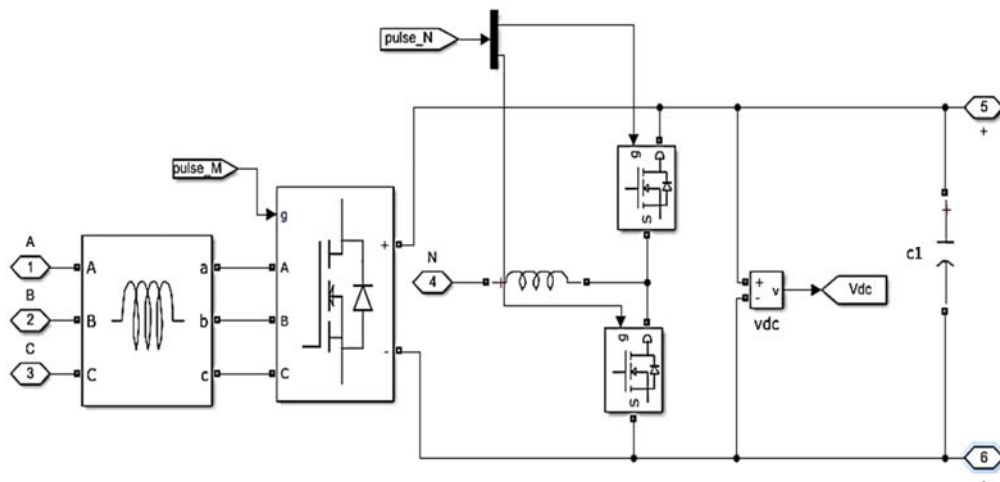


Figure 31: Voltage source inverter circuit model

The switching pulses for these power electronic switches are generated by using hysteresis controllers. The three-phase input current  $i_{abc}$  is transformed into  $i_{dq}$  using Park transform. The active current  $i_d$  is passed through a low pass filter to obtain the harmonic content. Park's transformation from the Dq0 reference frame to the ABC reference frame is used. After this transformation, the harmonic current is compared with the filter current using a hysteresis controller to produce the switching pulses of

the semiconductor switches (Purwadi et al., 2013). Figure 32 shows the block diagram of the filter control.

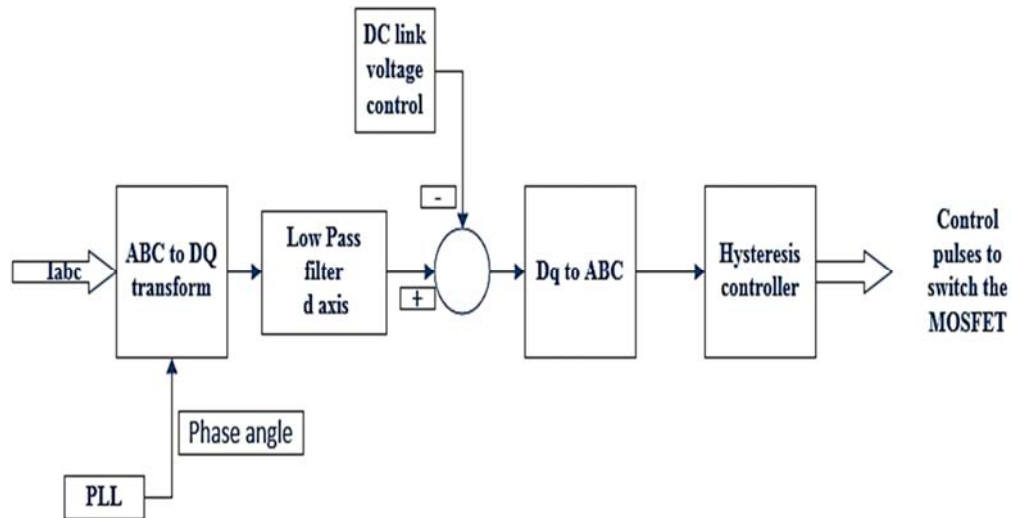


Figure 32: Filter control

After ABC transformation to dq0, the d axis contains an active power component of the load current, and the q axis contains a reactive power component. Using a low pass filter in the d axis extracts harmonic current content from the load current. A low pass filter is used to remove the fundamental current. The other q axis contains the reactive power component and negative sequence component of the load current. The detailed block diagram of this circuit configuration is shown in Figure 33 (Bhattacharya, Frank, Divan, & Banerjee, 1998).



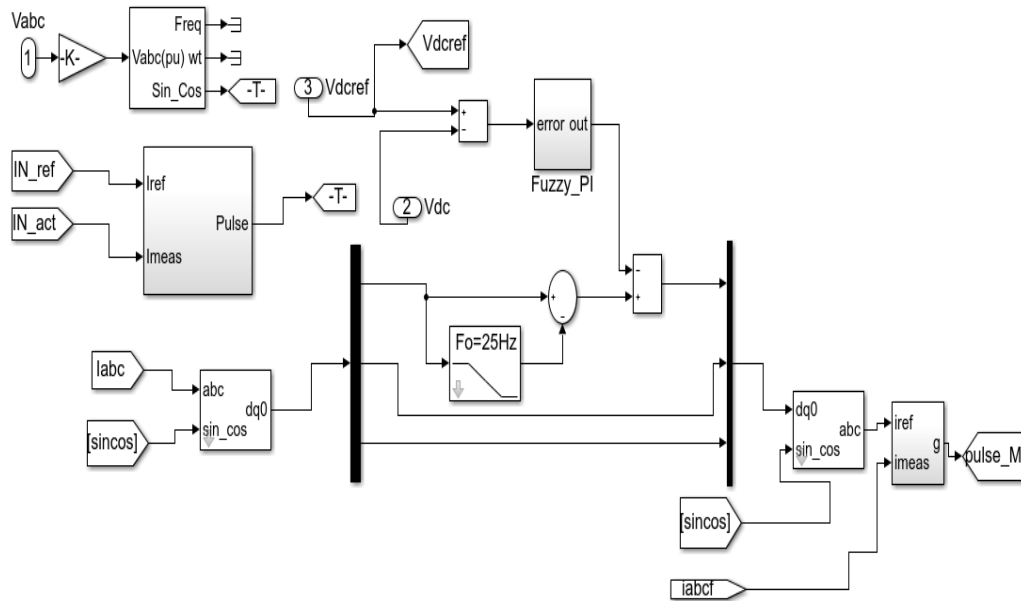


Figure 33: Connection diagram of positive sequence SRFC

The reference current includes the harmonic current, negative sequence current, and reactive power component of the load current. Inverse (dq0 to ABC) transformation is used to revert back to the three-phase quantities. Thus, this configuration successfully generates the reference current for the PAF. This circuit configuration results in harmonic-free phase and balanced current.

A similar operation is applied to the neutral conductor. During unbalanced condition the distorted currents pass through the common neutral, most of these higher frequency harmonics wave cancel out just like what we expect from the fundamental wave. Some harmonics, however, can not be cancelled. In fact, they add in the neutral. These harmonics are called zero sequence harmonics, and they are the reason for high neutral currents. This large current level can easily damage the neutral conductor, creating an open neutral environment with very serious consequences. To make up for this impact, the neutral current compensation is also introduced. Figure 34 shows the

circuit diagram of the neutral current compensation. The inductor connected to the load neutral point.

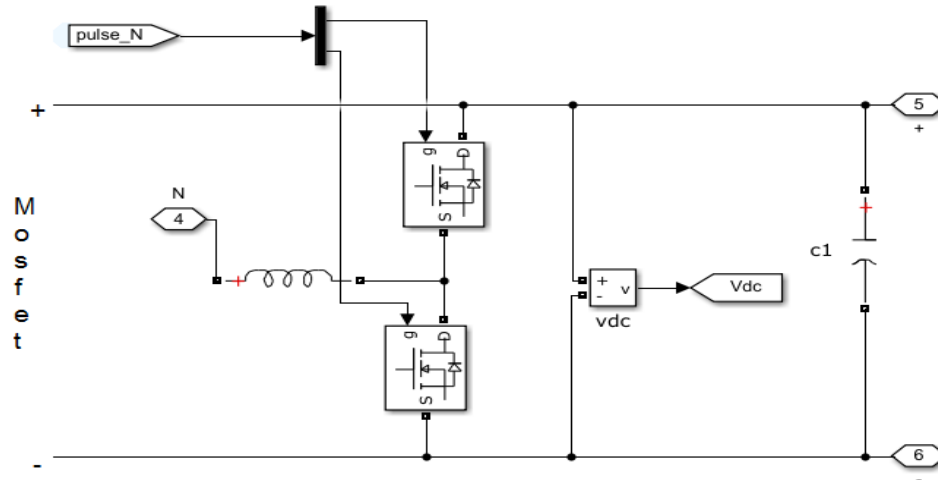


Figure 34: Connection diagram of neutral current compensation

## 2.6 DC link voltage control

The control algorithm of the PAF should also produce a reference current to regulate the DC link voltage to the DC bus reference voltage. Figure 35 shows the block diagram of the capacitor voltage control. A PI regulator is used to generate a reference current  $I_{Fdc}$  for the DC link voltage regulation. In deriving the mathematical model of the system, an experimental method via trial and error is used to obtain the gain of the PI controller.

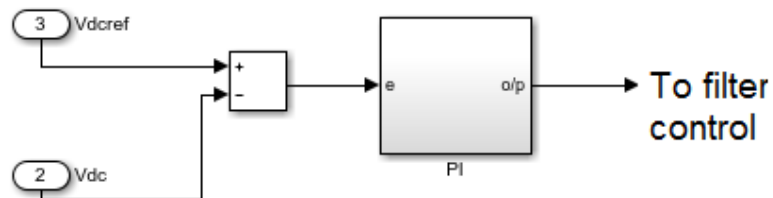


Figure 35: Capacitor voltage control

The bi-directional power flow of the MOSFET facilitates the harmonic current injection from the DC bus to the power grid. At the same time, the current flows to charge the capacitor from the grid side to the DC link. The reference voltage of the DC link for a three-phase bi-directional converter can be obtained by using  $\sqrt{2}V_s$ . Any value above  $\sqrt{2}V_s$  can be selected as the DC link reference voltage. Hence, the supply voltage is 415 V. Moreover, the  $\sqrt{2}V_s$  becomes 586 V. Furthermore, 700 V is selected as a reference voltage. This reference value is compared with a capacitor voltage. The obtained current reference from the DC bus voltage regulator is added to the d-axis current reference component of the harmonic current reference generator because the regulation of the DC bus voltage and compensation of the VSI losses require actual power transfer from the utility grid at the fundamental frequency.

In this model, the PI controller is used to control the DC link voltage. The THD of the system in the load side is 7.71%, as shown in Figure 36, and the THD decreases significantly to 3.5%, as shown in Figure 37, due to the effect of the VSI.

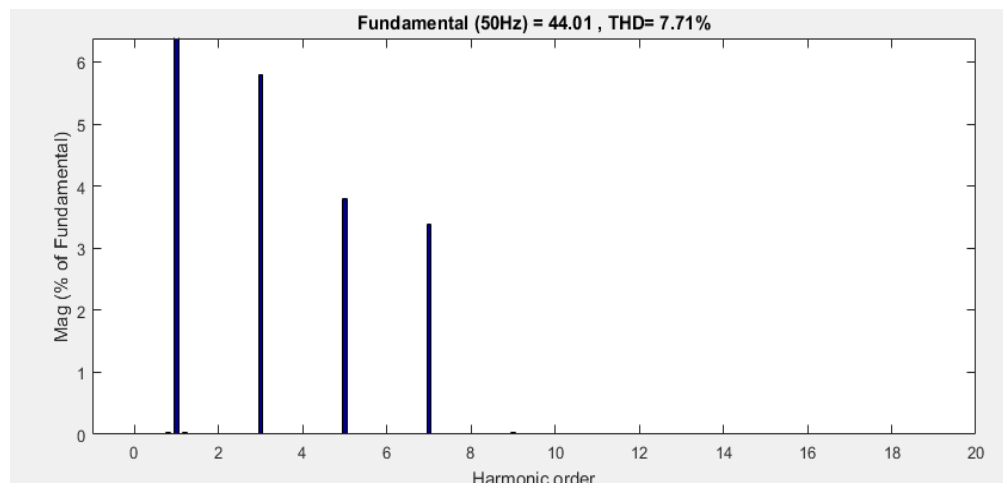


Figure 36: Load side THD

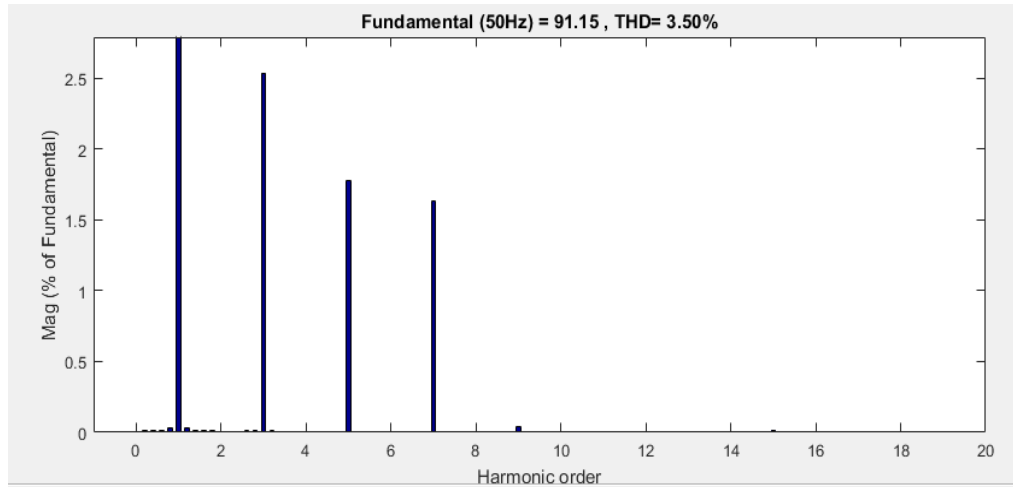


Figure 37: Source side THD

However, the tuning of the PI controller identifies the most suitable P and I values for the system. Thus, fuzzy logic is used for the self-tuning of the PI controller. A detailed explanation of the fuzzy logic and its implementation is provided in the following section.

## 2.7 Fuzzy PI controller

FLC is utilized to eliminate the reliance on PI controller and possible to tune the  $K_p$  and  $K_i$  values without knowing the exact mathematical model of the system. The self-tuning of the PI controller is realized in this work by using Fuzzy PI with two inputs and two outputs. The error and change of error between the DC link voltage and the reference voltage are used as the input to the fuzzy controller, and the values of  $k_{p1}$  and  $K_{i1}$  are the output. The author of (Ismail, 2012) Proposed a fuzzy self-tuning PID. However, in our model, only PI is used. Hence, the derivative section is excluded in the model.

### 2.7.1 Mamdani's method

One of the most common fuzzy inference techniques is called Mamdani's method. This method is widely applied to many fuzzy logic control systems given the use of min-max operations. The main idea of a Mamdani fuzzy inference system is to use fuzzy set theory to map an input to the output. In this technique, min is used as a conjunction operator, and max is used as an aggregation operator. Four steps are involved in these techniques, and they are explained as follows.

Step 1. Fuzzification - The first step determines the degree at which the crisp inputs belong to each of the fuzzy sets.

Step 2. Evaluation of fuzzy rules - Fuzzy operators, such as AND and OR, are used to obtain a single value that shows the results of antecedent evaluation. AND is used to evaluate the conjunction rule of the antecedent fuzzy operator, whereas fuzzy operator OR is used in the case of a disjunction of rule antecedents. The next step is to identify the combination of the rule strength and output MF to obtain the consequence of the rule.

Step 3. Aggregation - In this step, the consequences are combined to obtain a single fuzzy set.

Step 4. Defuzzification - To obtain the output as a single number and not as a fuzzy set, the obtained result from the previous step should be transformed into a single number. Many methods for defuzzification are available, and they include the centroid method for finding a point marking the center of gravity of an aggregated fuzzy set and the mean of maxima, in which the mean value of the maximum MFs is the output crisp value.

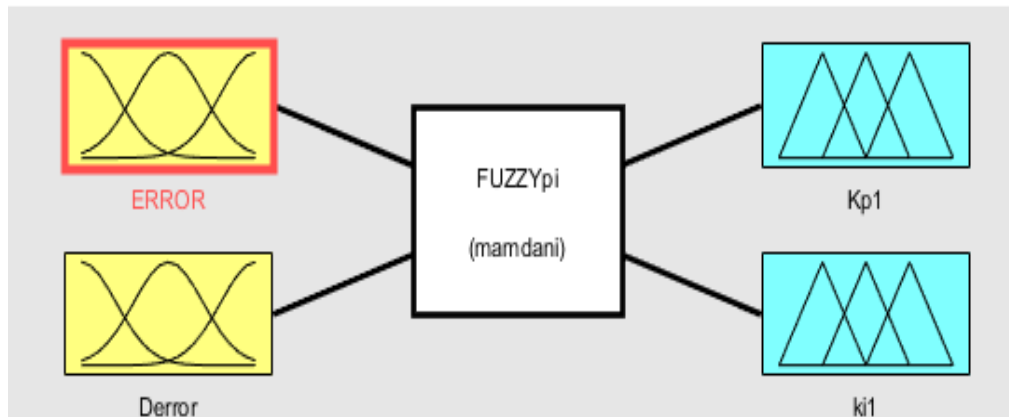


Figure 38: Block diagram of fuzzy PI

$$U_{pi} = K_{pnew} * e(t) + K_{inew} \int e dt \quad (2.14)$$

Block diagram of fuzzy PI is shown in Figure 38. Connection diagram of FLC to the filter model is also shown in Figure 39.

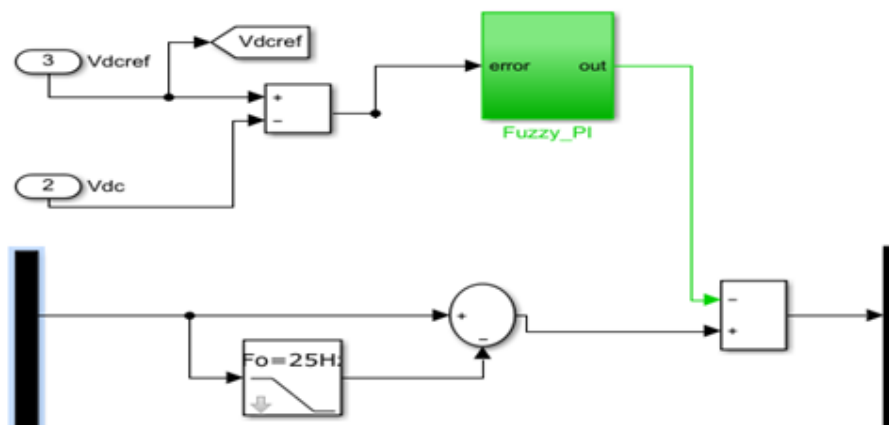


Figure 39: Fuzzy PI for DC link voltage control

$$K_{new} = K_{p1} * K_p \quad (2.15)$$

$$K_{inew} = K_{i1} * K_i \quad (2.16)$$

Where  $K_{new}$  and  $K_{inew}$  are the new gains of Fuzzy PI controller and  $k_{p1}$  and  $k_{i1}$  are the outputs of the gain of fuzzy controls,  $K_p$  and  $K_i$  are the initial PI values.

Tables 8 and 9 show the rule base used for the self-tuning of the fuzzy PI controller. The fuzzy control rule involves defining the relationship between the input error and the change of error in the output variables  $k_{p1}$  and  $k_{i1}$ . The rules are normally expressed by the if-then rule. If error  $e$  is “ $x$ ” and the change of error  $\Delta e$  is “ $y$ ”, then the output is “ $z$ ”. For enhanced performance and control, the input variable is modeled with seven triangular MFs, as shown in Figure 40. Figure 41 shows the MFs of  $K_{p1}$  and  $K_{i1}$ . The acronyms used are NB = negative Big, NM = negative medium, NS = negative small, ZE = zero error, PS = positive small, PM = positive medium, and PB = positive big. The output is also modeled using the triangular MF (VB, MB, B, M, S, MS, and ZE).

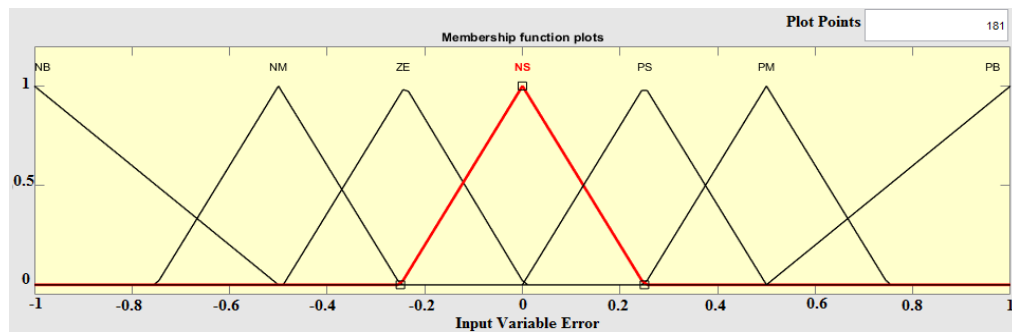


Figure 40: Membership function of inputs (error & change of error)

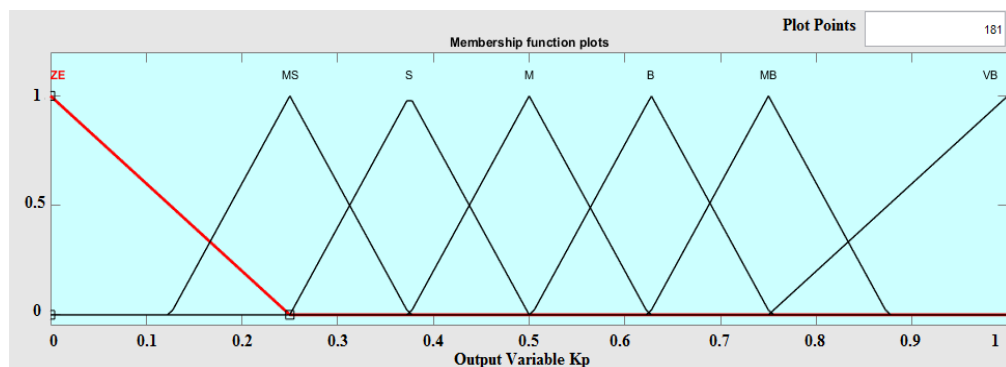


Figure 41: Membership function of outputs ( $K_{p1}$  and  $K_{i1}$ )

Table 8: Rule base for determining  $K_{p1}$ 

$\Delta e$ \ e	NB	NS	ZE	PS	PB
NB	VB	VB	VB	VB	VB
NS	B	B	B	MB	VB
ZE	ZE	ZE	MS	S	S
PS	B	B	B	MB	VB
PB	VB	VB	VB	VB	VB

Table 9: Table base for determining  $K_{i1}$ 

$\Delta e$ \ e	NB	NS	ZE	PS	PB
NB	M	M	M	M	M
NS	S	S	S	S	S
ZE	MS	MS	ZE	MS	MS
PS	S	S	S	S	S
PB	M	M	M	M	M

The fuzzy PI output is then fed to the d axis of the ABC to DQ transformation to obtain the reference current. This reference current is then fed to the hysteresis controller to produce the switching pulses. A detailed description of the hysteresis controller is presented in the following section.

## 2.8 Hysteresis controller

The performance of the current controller is important in obtaining a perfect compensation of harmonic currents. The switching pulses generated by the hysteresis controller are used to switch the MOSFETs. These switching circuits in the VSI reduce the DC link voltage to the required AC voltage at its output. One of the main



requirements of a hysteresis controller is that it should track high  $di/dt$  current references and distorted current waveforms. The hysteresis controller is proven as a current controller because of its high performance in tracking multiple frequencies and high  $di/dt$  currents.

The hysteresis band current control method is widely used for PWM due to the simplicity of implementation (Buso, Fasolo, Malesani, & Mattavelli, 2000). The main advantage of this controller is that it does not require any information about system parameters. It has rapid response and inherent peak current limiting capability. However, the switching frequency changes within the band due to the control of the peak-to-peak current ripple of the fundamental wave (Rodrigues, Schettino, Ferreira, Barbosa, & Braga, 2012).

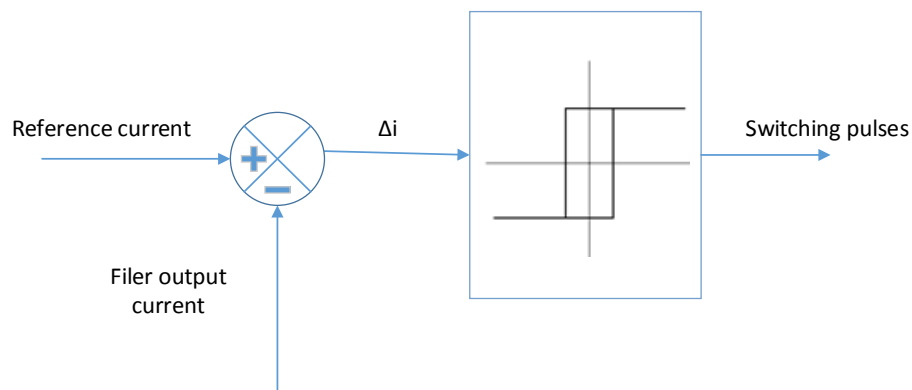


Figure 42: Hysteresis band controller

Figure 42 shows the operation of the hysteresis controller. The reference current, in this case, is the harmonic current, which should be injected to the grid for the harmonic current compensation. This current is compared with the filter output current, and the error current is  $\Delta i = i_r - i_f$ . If this value is greater than the tolerance,

then the current control of the active filter is initiated. If the error is between tolerances, then the position of the switch is preserved; otherwise, the switch on or off command is sent to the MOSFETS on the basis of the direction of the current error.

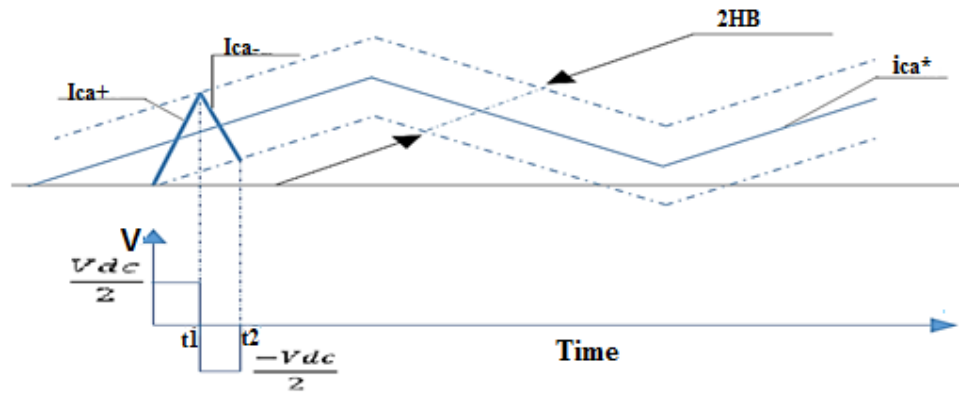


Figure 43: Hysteresis current control

$$T = t_1 + t_2 = \frac{1}{f} \quad (2.17)$$

From Figure 43, Where  $t_1$ ,  $t_2$  are switching intervals and  $f$  is the switching frequency.

The principle of hysteresis control is that when the output current of a VSI is greater than the hysteresis upper limit is  $+HB$ , the controller output becomes zero, the VSI output voltage is changed to  $= -V_{dc}/2$ , and the output current of the VSI decreases. Similarly, when the output current of the VSI is lesser than the hysteresis upper limit  $ir - HB$ , the controller output becomes zero, the VSI output voltage becomes  $= V_{dc}/2$ , and the output current of the VSI increases. Hence, the VSI output current can be controlled within the hysteresis band.

$$\frac{di_{ca}^+}{dt} = \frac{1}{L} (0.5V_{dc} - U) \quad (2.18)$$

$$\frac{di_{ca}^-}{dt} = -\frac{1}{L} (0.5V_{dc} + U) \quad (2.19)$$

From the geometry, we can say that

$$\frac{di_{ca}^+}{dt} t1 - \frac{di_{ca}^*}{dt} t1 = 2HB \quad (2.20)$$

$$\frac{di_{ca}^-}{dt} t2 - \frac{di_{ca}^*}{dt} t2 = -2HB \quad (2.21)$$

A pair of hysteresis controllers is utilized in each phase to calculate the phase current error. The circuit implementation of the hysteresis controller in each phase is shown in Figure 44. The figure shows that one pair of the controller is used in each phase. The corresponding switching pulses (g) in the circuit are fed to the gate terminal of the MOSFETs.

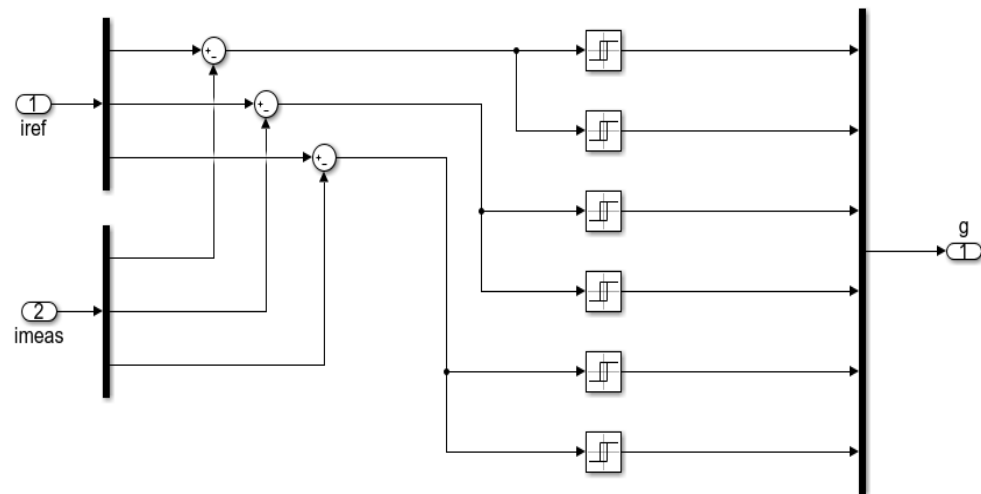


Figure 44: Hysteresis current regulator

### Chapter 3: Results and Discussion

A three-phase voltage source is used (415 V/50 Hz) to determine the performance of system operation. The loads in each phase are linear and nonlinear loads. A simulation is carried out in MATLAB/Simulink. Figure 45 shows the simulation result for the current waveform. The load comprising three equal resistors ( $R=5 \Omega$ ) and a nonlinear load injected as the current harmonic source are connected to each phase.

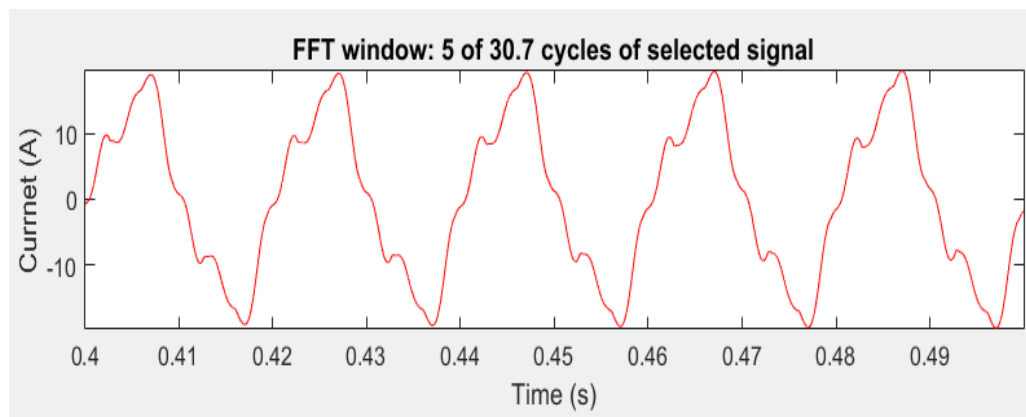


Figure 45: Load current waveform

Figure 46 shows the grid current waveform of the PAF connected to an EV charger. After active filtering with the conventional PI, the THD of the grid current waveform drops from 8.5% to 3.5% (Figure 47). This THD value is less than the allowable limit. Hence, these results show that the THDs generated by EV chargers can be successfully eliminated by using the PAF.

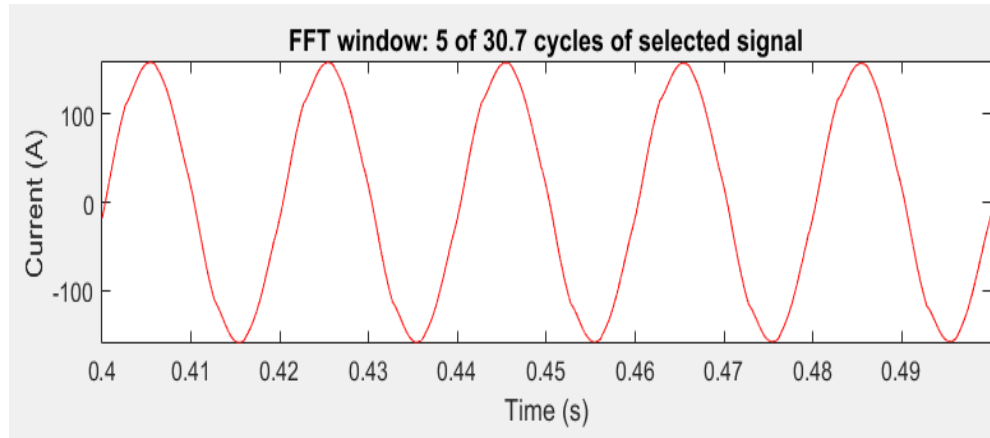


Figure 46: Grid current waveform of PAF with normal PI

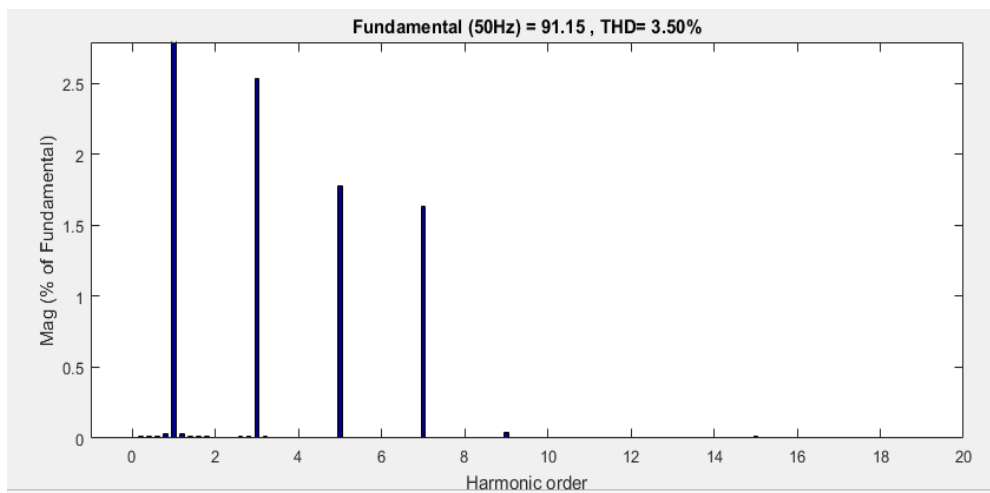


Figure 47: Grid current THD

Figure 48 shows the connection diagram of an active filter with a fuzzy PI connected parallel to the load circuit.  $V_{pcc}$  and  $V_{load}$  are the three-phase measurement block connected to the grid and load side respectively. The active filter is connected between these measurement block. The EV load is connected to the  $V_{load}$  measurement block through line impedance,  $R = 1\Omega$  and  $L = 0.001H$ . The harmonic content of this EV load is determined by using filter control shown in Figure 47. The output of filter

control is connected to the gate terminal of MOSFET in the filter converter. As shown in Figure 49, the gate pulse for neutral current and line current are pulse\_N and pulse\_M respectively. The inductor used in the active filter is used to reduce the ripple of VSI fed converters.

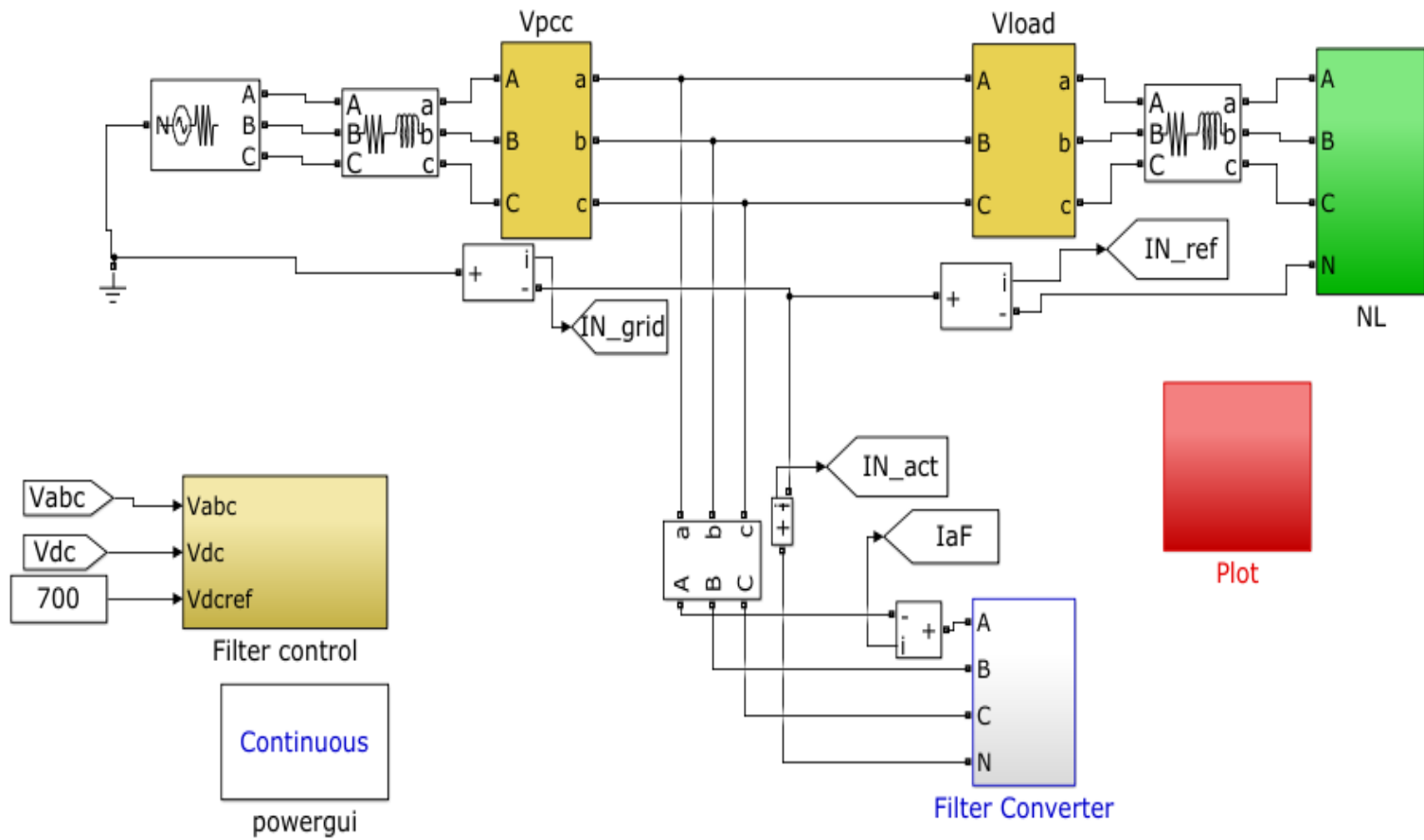


Figure 48: Connection diagram of EV load with VSI

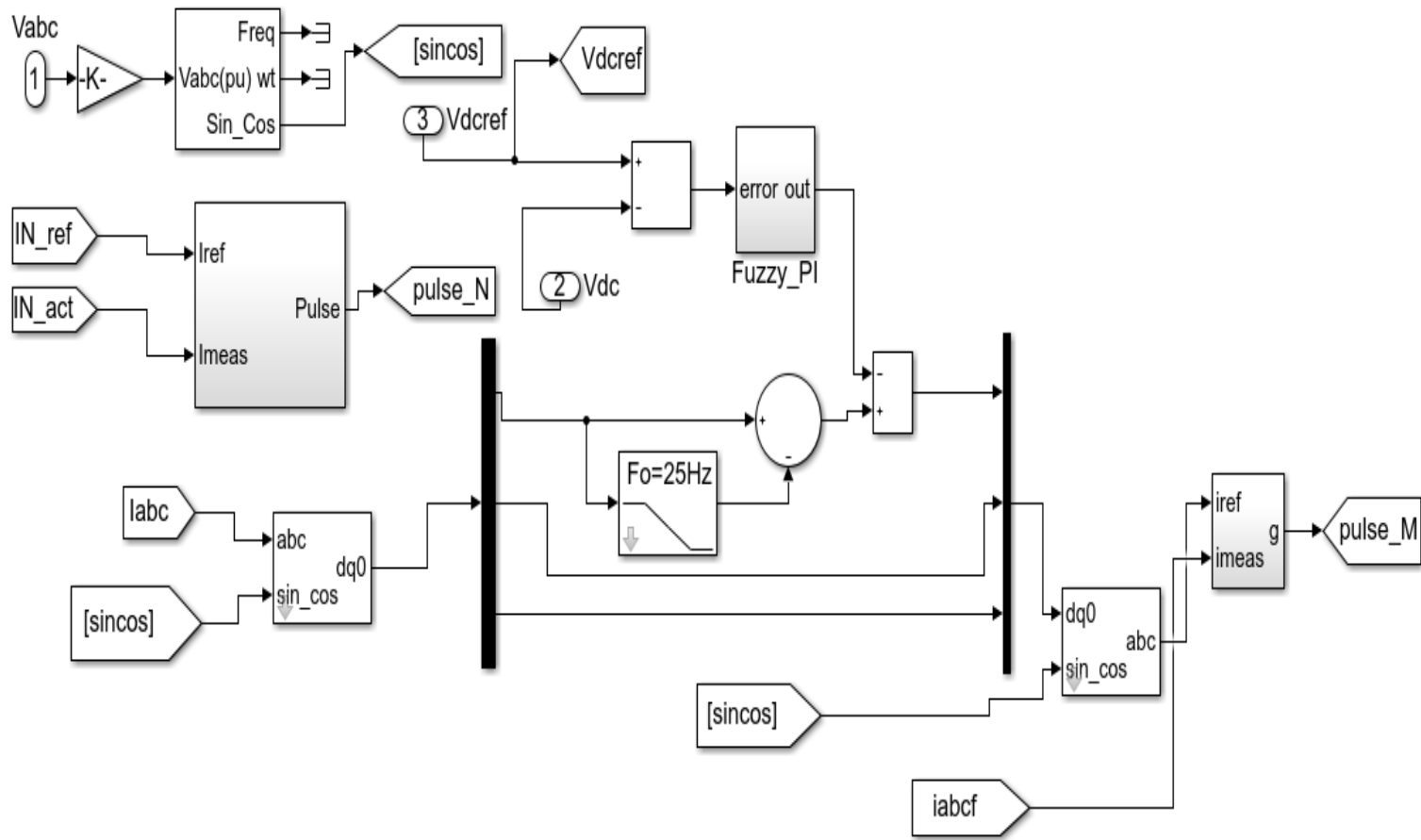


Figure 49: Filter control



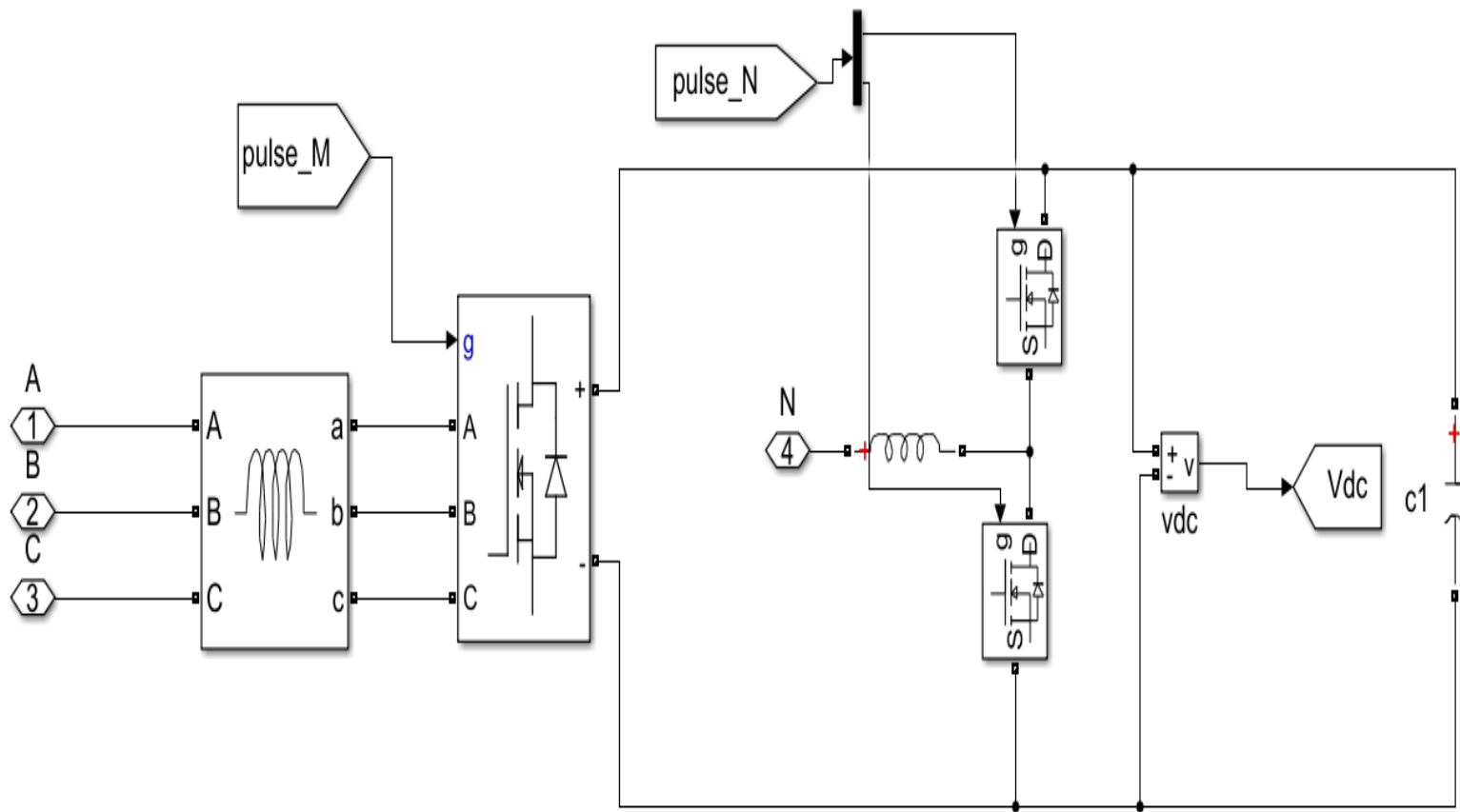


Figure 50: Filter converter

An active filter with a fuzzy PI is also simulated. A Mamdani min operator is used in the FLC. The error and change of error between the reference voltage and the DC link voltage are the input variables. Seven triangular MFs are used to obtain superior performance. The outputs of the FLC are  $k_{p1}$  and  $k_{i1}$ , which are further multiplied with the initial PI gain to obtain the fuzzy  $K_{p2}$  and  $K_{i2}$  values. These updated PI gains are used to control the DC link voltage. This method mitigates the harmonic distortion significantly in comparison with an active filter with a normal PI. Figure 51 depicts the current drawn from the grid at  $THDi = 1.40\%$ .

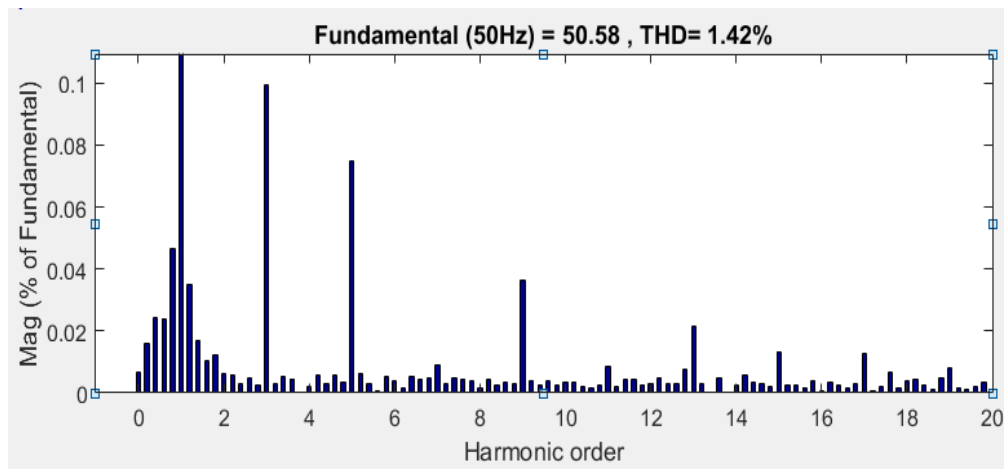


Figure 51: THDi of EV charger connected to VSI with fuzzy PI

If, for some reason, the DC link capacitor is discharged given that the EV charger is modeled using a bidirectional conduction mode, then smoothly recharging from the grid to the capacitor is possible. This charging process stops when the capacitor voltage reaches its reference value. Figure 52 shows the DC link voltage waveform during the startup.

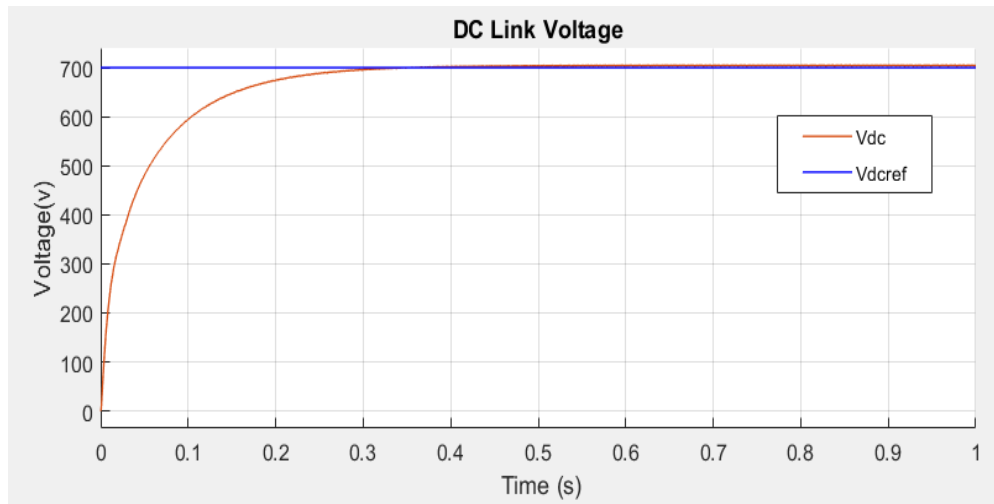


Figure 52: DC link voltage control

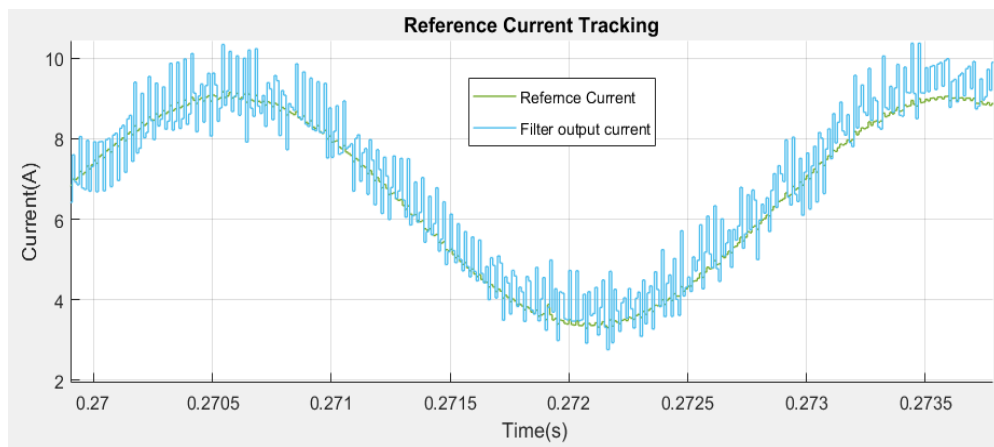


Figure 53: Reference current tracking

The reference current and filter current are shown in Figure 53. The figure evidently shows that the harmonic current is successfully tracked. The blue line indicates the reference current, and the varying signal across the reference current is the filter current.

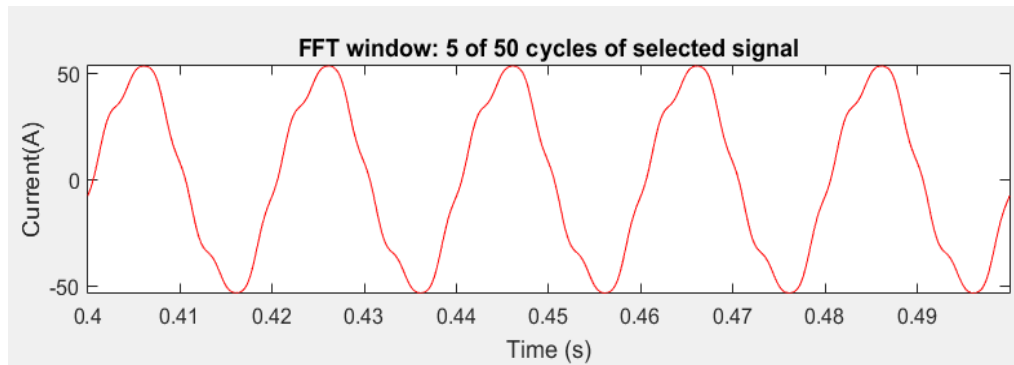


Figure 54: Load current waveform of PAF with fuzzy PI

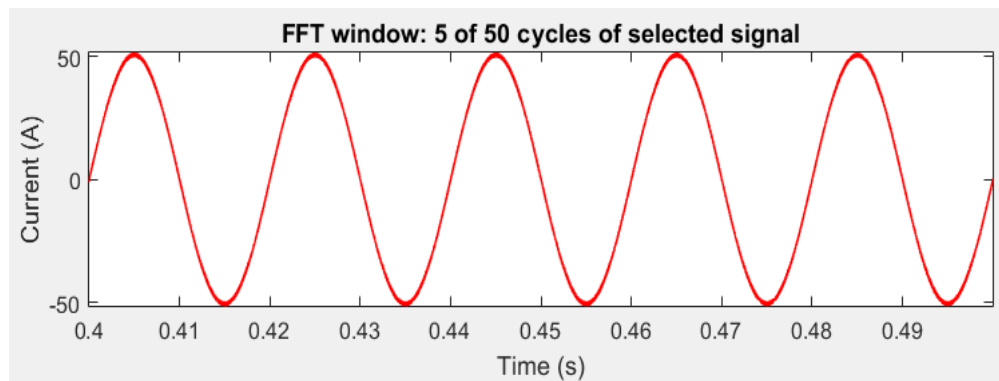


Figure 55: Grid current waveform of PAF with fuzzy PI

Figure 54 depicts the distorted waveform of the load current of the linear and nonlinear loads. The waveform clearly shows a distortion due to the presence of nonlinear loads. Figure 55 shows the grid current waveform. Evidently, the grid current is harmonic free. Most of the harmonic currents are compensated by the PAF.

### 3.1 Performance of VSI in various condition

The performance of the VSI when similar types of EVs are connected to the grid is discussed. The varying VSI performance during various operating conditions is important. These conditions include an additional EV connected to the R phase, two additional EVs connected to the R and Y phases, and the performance of the active

filter determined when a diode rectifier load is connected. Line current waveform, harmonic mitigation of active filter, and DC link voltage regulation during this condition are described in the following section.

*Case 1 – One additional EV plugged into R phase*

The current obtained by an EV charging station from the grid increases if an additional EV is plugged into the R phase. Hence, identifying the current harmonics generated by EVs, the THD mitigation of the modeled active filter, and DC link voltage control is highly important.

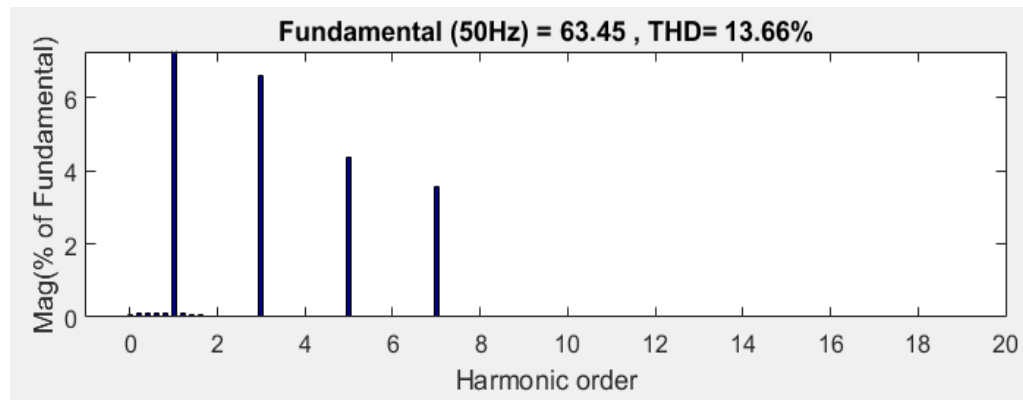


Figure 56: THDi at load side when an additional EV connected to R phase

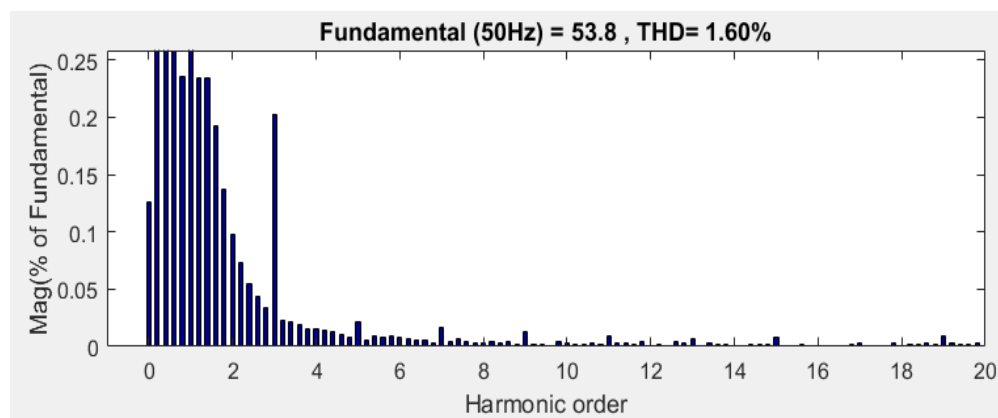


Figure 57: THDi at source side when an additional EV connected to R phase

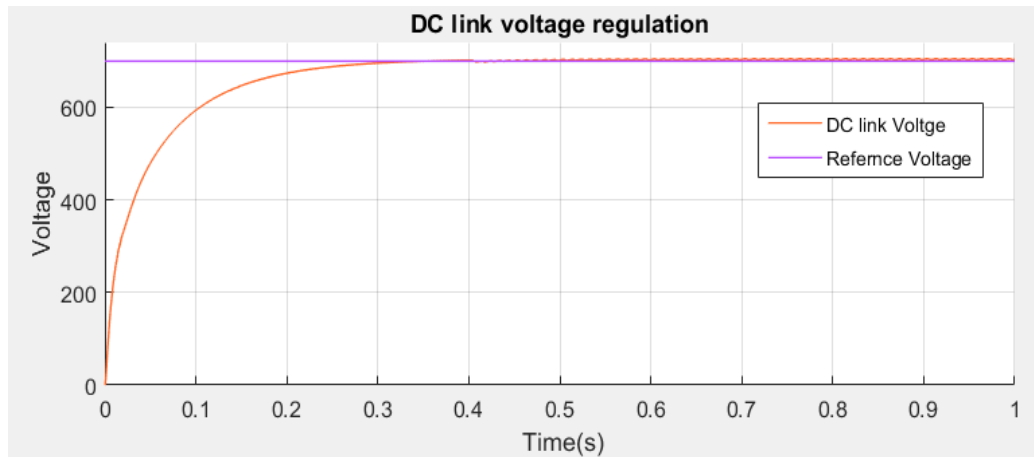


Figure 58: DC link voltage control when an additional EV plugged into R phase

Figure 56 and 57 show the THDi at the load side and source side, respectively. An additional EV is plugged to the grid after 0.4 s. As shown in the figure, the DC link voltage (Figure 58) regulation is also achieved after a short decay from the reference voltage. The neutral current is also tracked and well compensated to the circuit as shown in the Figure 59.

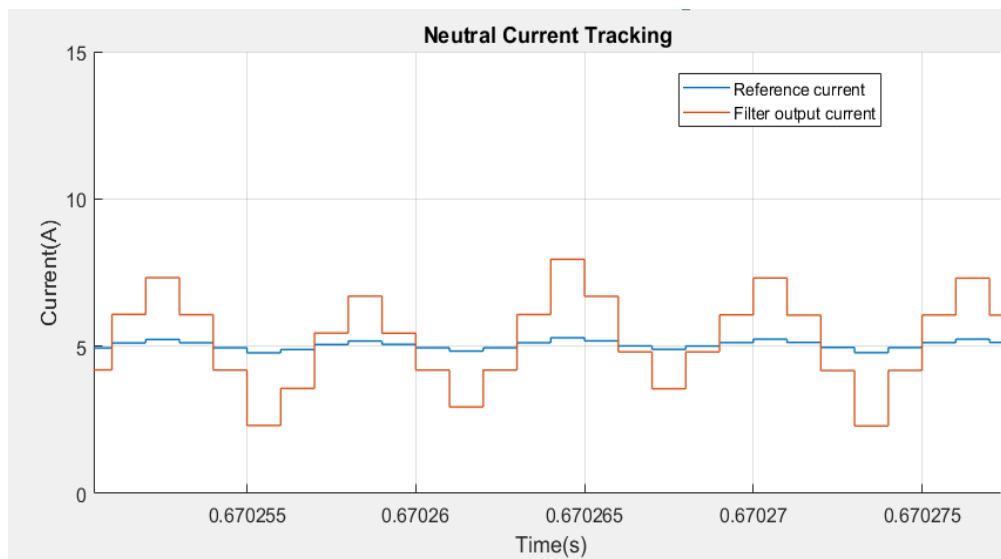


Figure 59: Neutral current compensation

*Case 2 – Two additional EVs plugged into R & Y phase*

Two additional EVs are plugged into the R and Y phases, respectively, after 0.45 second. Figure 62 shows that the DC link voltage drops by approximately 695 V due to the sudden load increase. However, due to the action of the FLC, the DC link voltage reverts back to the reference voltage after a short duration. Figure 60 and 61 shows the THDi at load side and source side respectively.

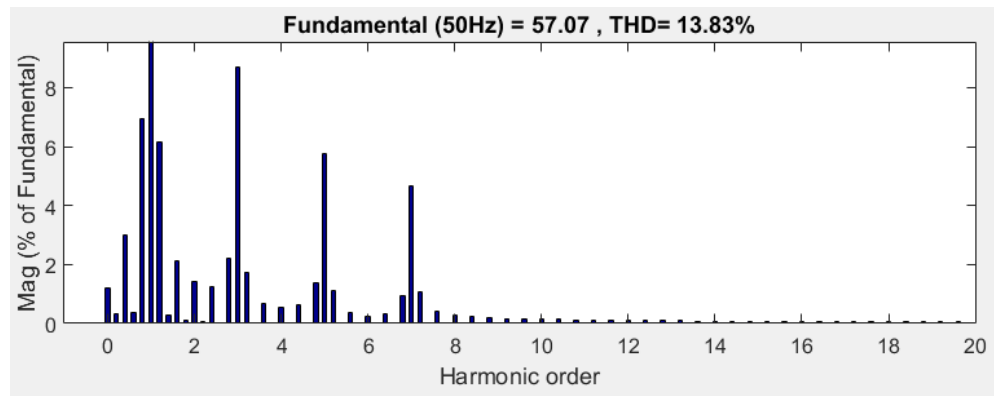


Figure 60: THDi at load side when two additional EVs are plugged into the system

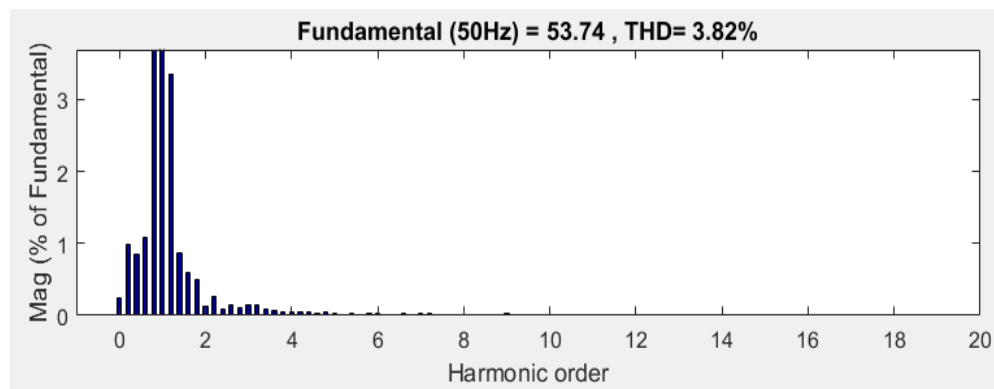


Figure 61: THDi at source side when two additional EVs are plugged into the system

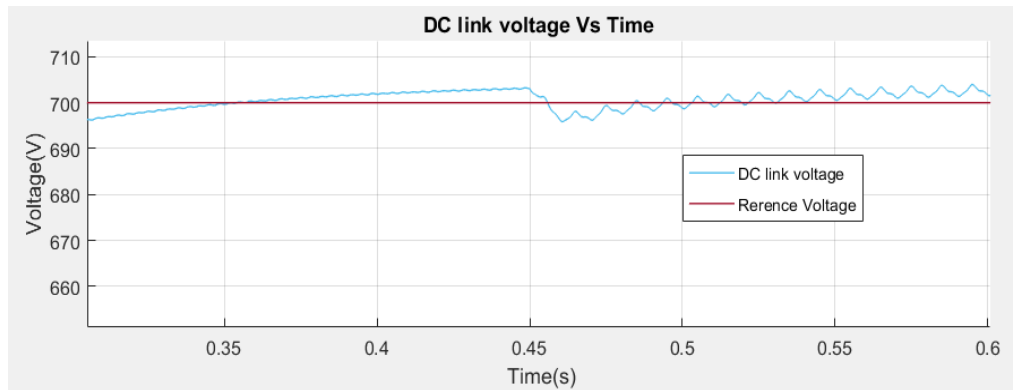


Figure 62: DC link voltage when two additional EVs are plugged at 0.45s

As shown in the figure, due to the addition of EVs, the DC bus voltage drops to approximately 5 V. However, due to the action of the FLC used in DC link voltage control, the DC link voltage to its reference voltage increases to approximately 0.5 s.

### Case 3 – Active filter connected to Diode rectifier

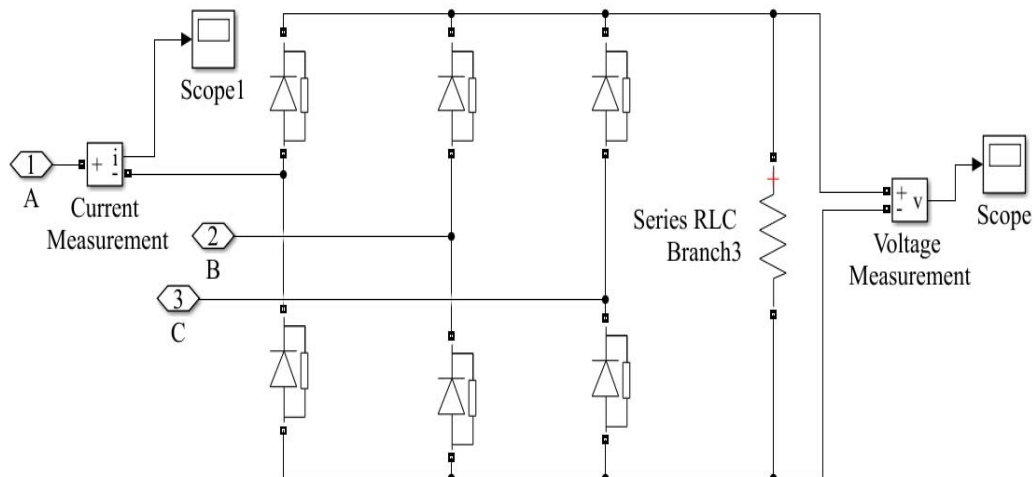


Figure 63: Diode rectifier connected to active filter

Another case study uses a diode rectifier as a nonlinear load Figure 63. In this case, the diode rectifier is connected instead of EVs. The DC link voltage, line current, and THDi at the load and source sides are analyzed. As expected, the THDi of the



diode filter is successfully reduced by the use of an active filter. The distorted grid current on the R phase is shown in Figure 64.

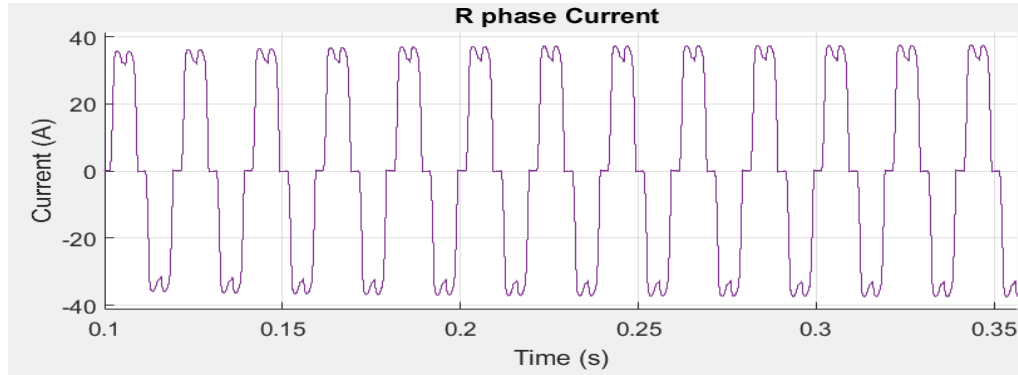


Figure 64: Current waveform on the R phase

The graph shows the DC link voltage. Figure 65 shows that the DC link voltage reaches its reference voltage of 0.7 s after start up. The THD drops from 7.98% (Figure 66) to 0.51% (Figure 67).

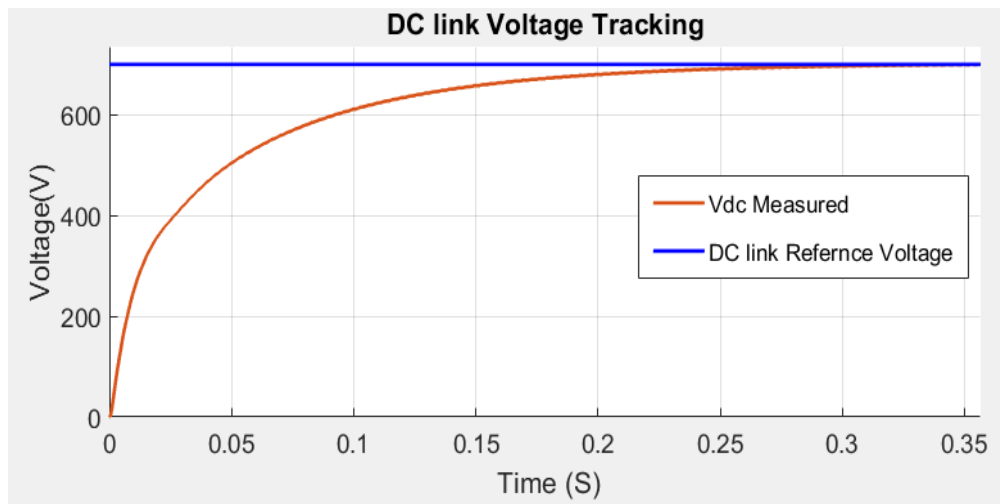


Figure 65: DC link voltage when diode rectifier connected

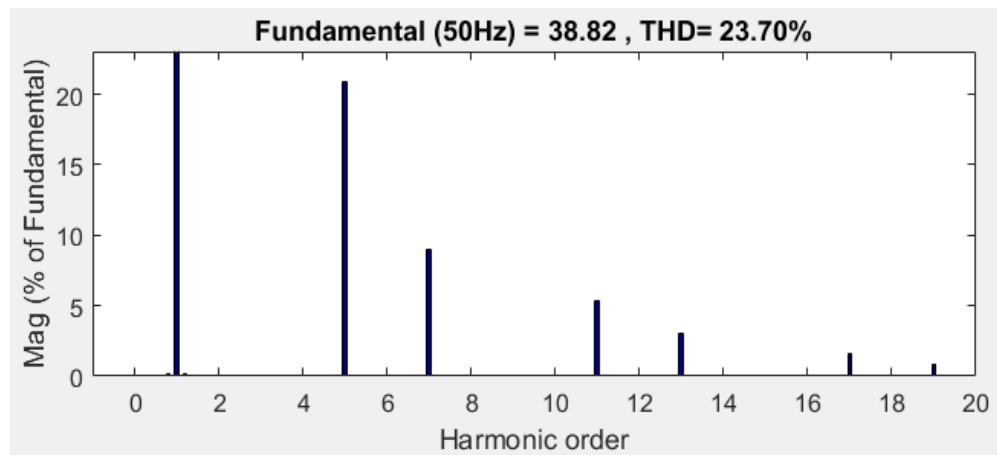


Figure 66: THDi at load side

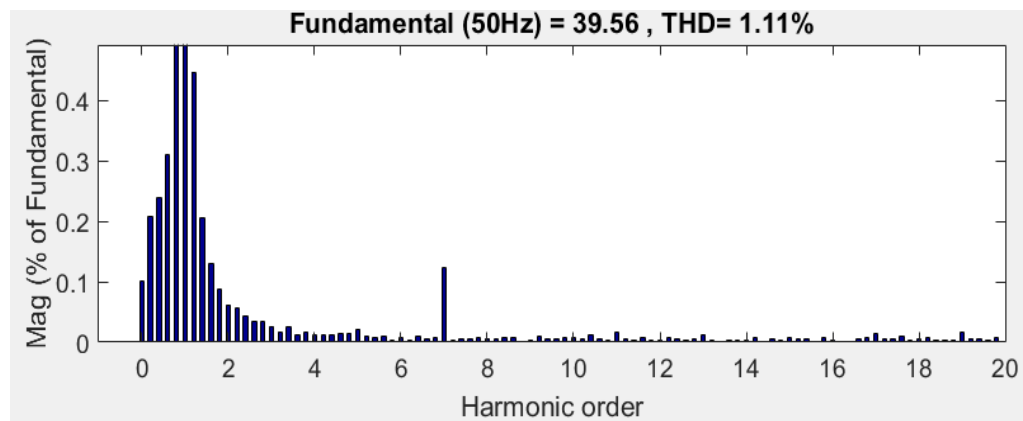


Figure 67: THDi at the grid side when diode rectifier connected

The performance of the VSI is as expected. The performance of harmonic mitigation in various scenarios is excellent. In addition to the FLC-based DC link, voltage control provides excellent control of DC link voltage regulation whenever the nonlinear load increases. Therefore, the modeled active filter is excellent in mitigating the harmonics in an EV charging station. Table 10 summarizes the performance of the EV charger in various scenarios.

Table 10: Comparison of the control strategy

Model Description	Current THD (%)	
	Load Side	Grid side
EV charger without any control	6.48 %	6.48 %
Active filter integrated to EV charger model with conventional PI	7.71 %	3.5 %
Active filter integrated to EV charger model with fuzzy PI	8.4 %	1.4 %
Case1 – One additional EV connected to R phase	13.66 %	1.60 %
Case1 – Two additional EVs connected to R, Y phase.	13.83 %	3.82 %
Case3 – Active filter connected to diode rectifier	23.7 %	1.11 %

## **Chapter 4: Conclusion**

A three-phase shunt active filter is developed using fuzzy logic and hysteresis controller to mitigate the current harmonics generated by EV chargers. An EV charger is modeled as an injected current harmonic source. The harmonic current content of the EV load is estimated using a positive sequence SRFC. The hysteresis band control technique is used to generate the switching pulses of MOSFETs. The conventional PI regulator is replaced with a fuzzy logic controller to provide excellent dynamic control of the DC link capacitor voltage at different operating conditions. The EV charger and active filter are developed and simulated using MATLAB/Simulink. The simulation results show that the performance of the active filter improves using fuzzy PI relative to the conventional PI controller. The active filter reduces the THDi of three similar EVs from 8.4% to 1.4%. Moreover, the THDi at the source side in various operating conditions is below the limits set by the IEEE 519-1992 harmonic standard.

## References

- Aiqiang Pan, Yongwei Zhu, Lijia Ren, Tiantian Chen, Sun Wen, & Wang Yun. (2016). Harmonic research of electric vehicle fast chargers. *2016 IEEE PES Asia-Pacific Power and Energy Engineering Conference (APPEEC)*, 2545–2549. <https://doi.org/10.1109/APPEEC.2016.7779947>
- Aljanad, A., & Mohamed, A. (2016). Harmonic Impact of Plug-In Hybrid Electric Vehicle on Electric Distribution System. *Modelling and Simulation in Engineering, 2016*, 1–7. <https://doi.org/10.1155/2016/5968943>
- Bhattacharya, S., Frank, T. M., Divan, D. M., & Banerjee, B. (1998). Active filter system implementation. *IEEE Industry Applications Magazine*, 4(5), 47–63. <https://doi.org/10.1109/2943.715508>
- Blooming, T. M., & Carnovale, D. J. (2006). Application of IEEE STD 519-1992 Harmonic Limits. *Conference Record of 2006 Annual Pulp and Paper Industry Technical Conference*, 1–9. <https://doi.org/10.1109/PAPCON.2006.1673767>
- Buso, S., Fasolo, S., Malesani, L., & Mattavelli, P. (2000). A dead-beat adaptive hysteresis current control. *IEEE Transactions on Industry Applications*, 36(4), 1174–1180. <https://doi.org/10.1109/28.855976>
- Colak, I., Bayindir, R., Kaplan, O., & Tas, F. (2010). DC Bus Voltage Regulation of an Active Power Filter Using a Fuzzy Logic Controller. *2010 Ninth International Conference on Machine Learning and Applications*, 692–696. <https://doi.org/10.1109/ICMLA.2010.165>
- Deilami, S. (2018). Online Coordination of Plug-In Electric Vehicles Considering Grid Congestion and Smart Grid Power Quality. *Energies*, 11(9), 2187-2193. <https://doi.org/10.3390/en11092187>
- Fujita, H., & Akagi, H. (1998). The unified power quality conditioner: the integration of series- and shunt-active filters. *IEEE Transactions on Power Electronics*, 13(2), 315–322. <https://doi.org/10.1109/63.662847>
- Guo, J., Zhao, H., Shen, Z., Wang, A., Cao, L., Hu, E., ... Song, X. (2018). Research on Harmonic Characteristics and Harmonic Counteraction Problem of EV Charging Station. *2018 2nd IEEE Conference on Energy Internet and Energy System Integration (EI2)*, 1–5. <https://doi.org/10.1109/EI2.2018.8582095>
- Ismail, M. M. (2012). *Adaptation of PID Controller using AI Techniques for Speed Control of Isolated Steam Turbine*. 8.

- Kaiwart, J., & Raju, U. P. B. (2016). *Harmonic Mitigation Techniques: A Review*. 5(11), 8346 -8352.
- Kutt, L., Saarijarvi, E., Lehtonen, M., Molder, H., & Niitsoo, J. (2013). Current harmonics of EV chargers and effects of diversity to charging load current distortions in distribution networks. 2013 International Conference on Connected Vehicles and Expo (ICCVE), 726–731. <https://doi.org/10.1109/ICCVE.2013.6799884>
- Lee, C.-S., Jeong, J.-B., Lee, B.-H., & Hur, J. (2011). Study on 1.5 kW battery chargers for neighborhood electric vehicles. *2011 IEEE Vehicle Power and Propulsion Conference*, 1–4. <https://doi.org/10.1109/VPPC.2011.6043129>
- Melo, N., Mira, F., de Almeida, A., & Delgado, J. (2011). Integration of PEV in Portuguese distribution grid: Analysis of harmonic current emissions in charging points. *11th International Conference on Electrical Power Quality and Utilisation*, 1–6. <https://doi.org/10.1109/EPQU.2011.6128893>
- Nikoomanesh, M., Alizadehe, M., Naderi, P., & Soltani, I. (2014). *Series Active Filter Control with A Novel Load Voltage Harmonic Extraction Method*. 3(1), 46-50.
- Peng, F. Z. (2001). Harmonic sources and filtering approaches. *IEEE Industry Applications Magazine*, 7(4), 18–25. <https://doi.org/10.1109/2943.930987>
- Purwadi, A., Shani, N., Heryana, N., Hardimasyar, T., Firmansyah, M., & Sr, A. (2013). Modelling and Analysis of Electric Vehicle DC Fast Charging Infrastructure Based on PSIM. *2013 1st International Conference on Artificial Intelligence, Modelling and Simulation*, 359–364. <https://doi.org/10.1109/AIMS.2013.66>
- Rodrigues, M. C. B. P., Schettino, H. J., Ferreira, A. A., Barbosa, P. G., & Braga, H. A. C. (2012). Active power filter operation of an electric vehicle applied to single-phase networks. *2012 10th IEEE/IAS International Conference on Industry Applications*, 1–8. <https://doi.org/10.1109/INDUSCON.2012.6451796>
- Routimo, M., Salo, M., & Tuusa, H. (2005). Comparison of Voltage-Source and Current-Source Shunt Active Power Filters. *IEEE 36th Conference on Power Electronics Specialists*, 2571–2577. <https://doi.org/10.1109/PESC.2005.1581995>
- Shao, S., Pipattanasomporn, M., & Rahman, S. (2011). Demand Response as a Load Shaping Tool in an Intelligent Grid With Electric Vehicles. *IEEE Transactions on Smart Grid*, 2(4), 624–631.

- Singh, B., Singh, S., Chandra, A., & Al-Haddad, K. (2011). Comprehensive Study of Single-Phase AC-DC Power Factor Corrected Converters With High-Frequency Isolation. *IEEE Transactions on Industrial Informatics*, 7(4), 540–556. <https://doi.org/10.1109/TII.2011.2166798>
- Ul-Haq, A., Perwaiz, A., Azhar, M., & Ullah Awan, S. (2018). Harmonic Distortion in Distribution System Due to Single-Phase Electric Vehicle Charging. *2018 2nd International Conference on Green Energy and Applications (ICGEA)*, 205–209. <https://doi.org/10.1109/ICGEA.2018.8356277>
- Usman, H., Hizam, H., & Mohd Radzi, M. A. (2013). Simulation of single-phase shunt active power filter with fuzzy logic controller for power quality improvement. *2013 IEEE Conference on Clean Energy and Technology (CEAT)*, 353–357. <https://doi.org/10.1109/CEAT.2013.6775655>
- Wenjin Dai, Baofu Wang, & Hua Yang. (2009). A hysteretic current controller for active power filter with constant frequency. *2009 IEEE International Conference on Computational Intelligence for Measurement Systems and Applications*, 86–90. <https://doi.org/10.1109/CIMSA.2009.5069924>
- Yilmaz, M., & Krein, P. T. (2012). Review of charging power levels and infrastructure for plug-in electric and hybrid vehicles. *2012 IEEE International Electric Vehicle Conference*, 1–8. <https://doi.org/10.1109/IEVC.2012.6183208>
- Yilmaz, M., & Krein, P. T. (2013). Review of Battery Charger Topologies, Charging Power Levels, and Infrastructure for Plug-In Electric and Hybrid Vehicles. *IEEE Transactions on Power Electronics*, 28(5), 2151–2169. <https://doi.org/10.1109/TPEL.2012.2212917>